dermatomyositis muscle, myofibre injury is apparent in two forms: large areas of apparent infarction visible as the loss of myofibrillar uptake of multiple histochemical stains, seen occasionally in juvenile dermatomyositis and rarely in adult dermatomyositis, and the presence of perifascicular atrophy (PFA). PFA is a term used to describe small, basophilic myofibres around the edges of muscle fascicles. PFA does not generally affect all myofibres around the edge of the fascicle, but rather usually affects the specific myofibres that border the loose connective tissue (the perimysium), sparing myofibres that border other myofibres in neighbouring fascicles. The lesion is better described by the term perimysial PFA,[1,2] or even perimysial myofibre atrophy.

In dermatomyositis skin, the characteristic pathology is an interface dermatitis, in which abnormalities are most prominent at the boundary between the epidermis and dermis. It is characterized by the presence of dying keratinocytes centred mostly on those in the basal layer, in opposition to the underlying basement membrane. The more differentiated cells that are located higher in the stratum spinosum or stratum granulosum are rarely affected. This cell death is manifested by cells with pyknotic nuclei and eosinophilic cytoplasm as well as by vacuolization of the basal layer. Curiously, the dying cells are often not confluent, and are present in patchy foci often in association with infiltrating mononuclear cells. Epidermal atrophy is also seen in long-standing lesions.

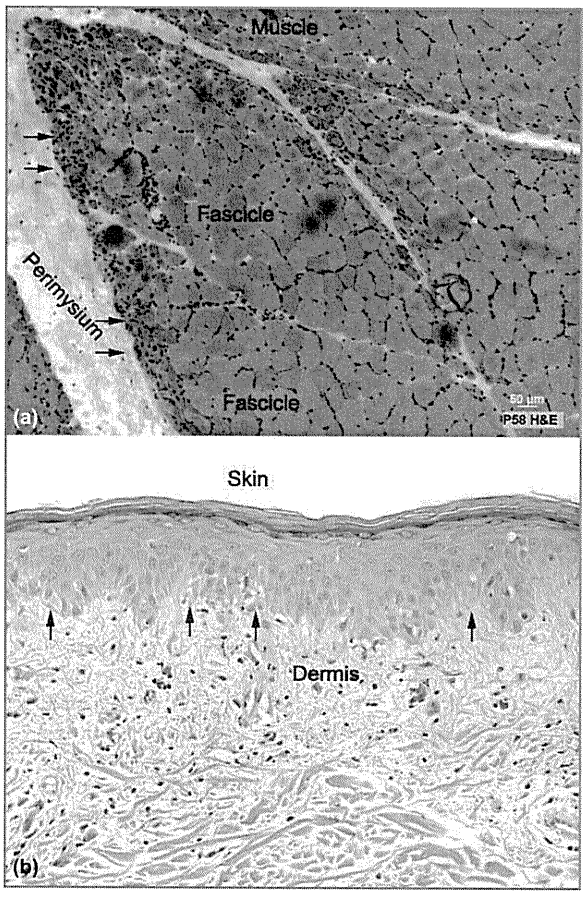

Fig 1. (a) Perimysial perifascicular atrophy in muscle. Small, basophilic fibres at the interface between myofibres and perimysial connective tissue (black arrows). (b) Interface dermatitis in skin. Vacuolated and degenerating keratinocytes at the interface between keratinocytes and loose connective tissue (black arrows). H&E, haematoxylin and eosin.

We point out here that the topology of the injury to both myofibres and keratinocytes is similar in dermatomyositis muscle and skin (Fig. 1). In both cases, injury preferentially affects the cells that border the loose connective tissue adjacent to them, with relative sparing of cells that are entirely surrounded by other cells. In cases with greater severity of changes, the pathology extends into deeper regions of muscle fascicles and more superficial layers of keratinocytes. Why such muscle and skin cells bordering loose connective tissue are more susceptible to injury is unknown. One speculative possibility is that these bordering cells are closer to cells of the immune system and their secreted products. It is possible that the pattern of muscle inflammation in dermatomyositis represents the 'muscle equivalent' of a lichenoid tissue reaction in the skin. Indeed, in this disease the inflammatory cells are usually much more abundant in muscle in the perimysial connective tissue than within fascicles, as they are more commonly seen in the papillary dermis and dermoepidermal junction than within the more superficial keratinocyte layers.

Department of Neurology, Brigham and Women's Hospital, Harvard Medical School, Boston, MA 02458, U.S.A.
S.A. Greenberg
D. Fiorentino*
*Department of Dermatology, Stanford University School of Medicine, Stanford, CA 94305, U.S.A.
E-mail: sagreenberg@partners.org

References

1 Carpenter S, Karpati G, Rothman S, Watters G. The childhood type of dermatomyositis. Neurology 1976; **26**:952–62.
2 Greenberg SA. Proposed immunologic models of the inflammatory myopathies and potential therapeutic implications. Neurology 2007; **69**:2008–19.

Key words: dermatomyositis, interface dermatitis

Conflicts of interest: none declared.

Morphological and genetic analysis of steatocystoma multiplex in an Asian family with pachyonychia congenita type 2 harbouring a *KRT17* missense mutation

DOI: 10.1111/j.1365-2133.2008.08983.x

Sir, Pachyonychia congenita (PC) is a rare, autosomal dominant keratin disorder. PC can be classified into two main clinical subtypes: PC type 1 (PC-1, OMIM 167200) and PC type 2

(PC-2, OMIM 167210). PC-1 is associated with mutations in *KRT6A* or *KRT16*, and PC-2 corresponds to mutations in *KRT6B* or *KRT17*.[1,2] Almost all mutations detected in patients with PC occur in the helix boundary motifs of each keratin gene.[3] Common clinical features of both PC subtypes are hypertrophic nail dystrophy, and focal hyperkeratosis of the palms, soles, knees and elbows.[4] Among clinical manifestations in patients with PC, the development of steatocystoma multiplex is one of the most characteristic features for differentiating PC-2 from PC-1. Typically, patients with PC-2 exhibit 100–2000 round or oval cysts widely distributed on the back, anterior trunk, arms, scrotum and thighs.

We report an Asian PC-2 family with a missense mutation in *KRT17*. In this study, we present histological and ultrastructural features of a steatocystoma from the proband. Furthermore, comparative analysis of genomic DNA (gDNA) extracted from steatocystomas and peripheral blood of the family was performed. These observations could provide significant information for understanding the pathomechanisms of cyst formation in patients with PC-2.

The proband was a 36-year-old Asian woman with the chief complaint of nail dystrophy. Natal teeth were observed at birth. During childhood, nail hypertrophy was seen on the toenails and fingernails (Fig. 1a). Follicular hyperkeratosis on the knees and elbows was also noted at puberty, although the symptom disappeared as she grew older. She also complained of focal hyperkeratosis on the soles. On the axillae, several subcutaneous cysts were observed (Fig. 1b). The proband's 3-year-old daughter had follicular keratosis on the knees, nail deformity, pilosebaceous cysts on the face, and focal hyperkeratosis on the soles. The proband's 62-year-old father had had nail dystrophy, numerous steatocystomas on the trunk and hyperkeratosis on the soles since his adolescence. The family has a strong genetic background of nail hypertrophy and steatocystoma multiplex (Fig. 1c).

gDNA was extracted from whole blood samples of the proband, her father and her daughter. *KRT6B* and *KRT17* were amplified from their gDNA by polymerase chain reaction (PCR) using specific primers to amplify the helix boundary motifs of each gene without coamplification of the pseudogenes and isogenes.[5,6] Mutation analysis for *KRT6B* showed no mutations of the gDNA, and analysis of *KRT17* indicated that the proband was a heterozygote for a recurrent mutation of c.296T>C transition (p.Leu99Pro) in *KRT17* (Fig. 1d). The father and daughter were also heterozygotes for the same mutation in *KRT17*. Restriction enzyme digestion of PCR products by NciI was carried out to confirm the mutation (data not shown). The mutation was not found in 50 normal control individuals. This mutation was previously reported elsewhere.[2,7]

Histopathological findings of skin specimens from a steatocystoma of the proband showed that the cyst wall consisted of several thin epithelial cell layers without granular layers (Fig. 2a,b). There were sebaceous glands near the cyst wall (Fig. 2b). Large basophilic granules were scattered in the cytoplasm of the uppermost-layer cells in the cyst walls (Fig. 2c). Immunohistochemically, upper layer cells in the cyst wall expressed keratin 17 (Fig. 2d). Ultrastructural observation revealed keratin clumps in the cytoplasm of epithelial cells in the cyst wall (Fig. 2e). The keratin clumps were large and irregularly shaped (Fig. 2f).

We excised one steatocystoma and overlying epidermis from the proband and three steatocystomas from the proband's father, and we removed the normal tissue of the steatocystomas and intracystic materials as much as possible. DNA was extracted from both the cyst wall of steatocystomas and the overlying epidermis. Direct sequencing of gDNA from all

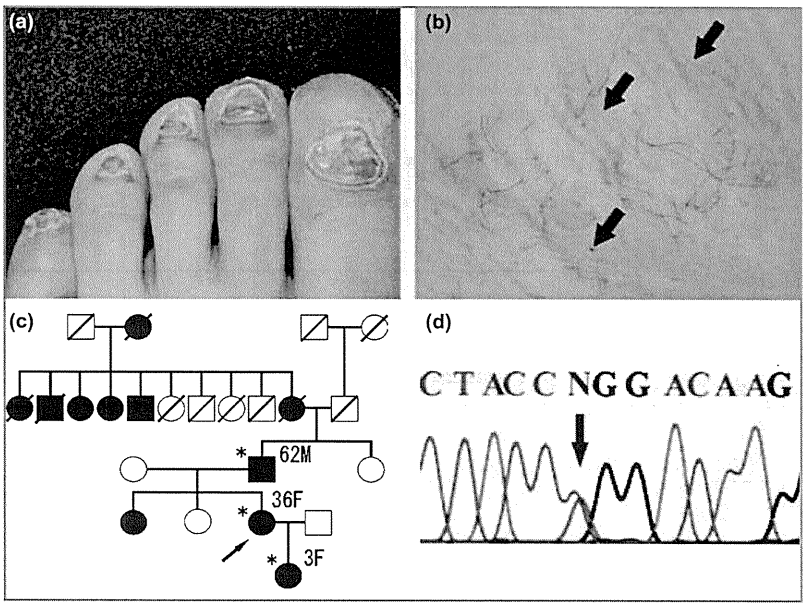

Fig 1. Clinical features of the proband, pedigree of the present family and mutation analysis of *KRT17*. (a) The proband's toenails showed severe dystrophy. (b) There were several steatocystomas on the proband's axillae (arrows). (c) The family history indicated strong penetrance. Squares indicate males, and circles, females. Blackened symbols are individuals with pachyonychia congenita type 2. The proband is indicated by an arrow. The asterisks indicate individuals who underwent mutation analysis. (d) Direct DNA sequence analysis of the helix initiation motif in *KRT17*; the c.296T>C transition mutation (p.Leu99Pro) in one allele of *KRT17* was found in the proband's blood.

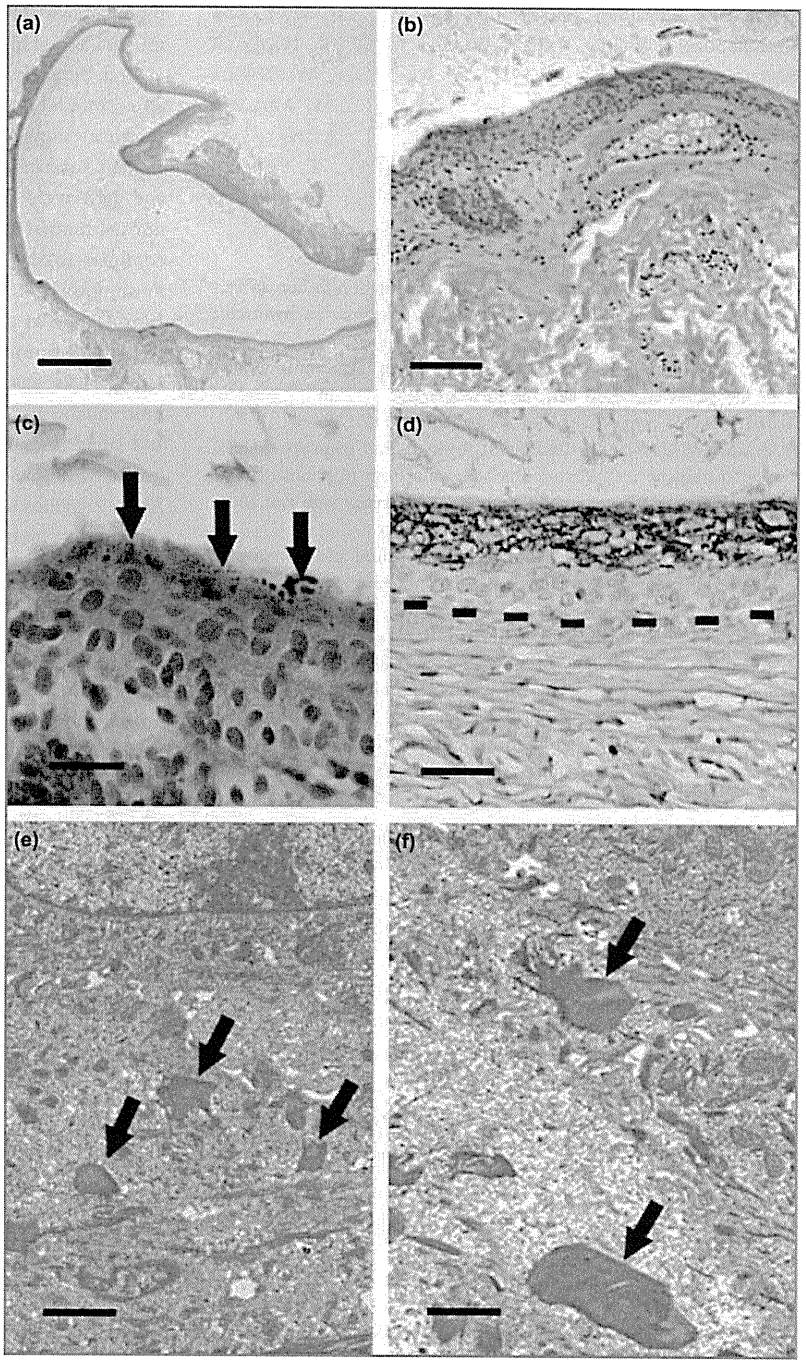

Fig 2. Histological and ultrastructural findings of a steatocystoma from the proband. (a) There were sebaceous glands near the cyst wall (haematoxylin and eosin; bar = 1·2 mm). (b) The cyst wall was composed of several epithelial cell layers (haematoxylin and eosin; bar = 100 μm). (c) Large basophilic granules (arrows) were present in upper layer cells in the cyst wall (haematoxylin and eosin; bar = 20 μm). (d) Immunohistochemical examination was performed using primary antibody, mouse monoclonal antibody E3 recognizing keratin 17 (K17). K17 was expressed in the upper layer cells in the cyst wall. Dotted line: epithelial–mesenchymal junction (bar = 50 μm). (e) There were keratin clumps in the cytoplasm of epithelial cells in the cyst wall (arrows) (bar = 2 μm). (f) The keratin clumps (arrows) were large and irregularly shaped (bar = 1 μm).

samples identified the same KRT17 mutation in one allele as seen in the family's peripheral blood (data not shown). Comparative sequence analyses for helix boundary motifs of KRT6B and KRT17 on gDNA extracted from the cyst wall and overlying epidermis vs. gDNA isolated from whole blood samples revealed neither sequence deviations indicative of loss of heterozygosity (LOH) nor second-hit mutations (data not shown).

Our results for four steatocystomas from patients with PC-2 suggest that cyst formation does not require a complete functional loss of keratin. The absence of LOH or second-hit mutations indicates that steatocystoma multiplex comprises benign cysts rather than tumours. Notably, the cyst wall of the steatocystoma from the proband had large basophilic granules. Ultrastructural observation confirmed that the granules were keratin clumps, which resulted from the conformational change in keratin filaments due to the KRT17 mutation. Dominant negative effects from a mutation in KRT17 may be sufficient to cause steatocystomas in patients with PC, although the exact mechanisms of steatocystoma formation remain unclear.

Department of Dermatology, Hokkaido University Graduate School of Medicine, North 15 West 7, Sapporo 060-8638, Japan
Correspondence: Ken Natsuga.
E-mail: natsuga@med.hokudai.ac.jp

M. Kanda
K. Natsuga
W. Nishie
M. Akiyama
A. Nagasaki
T. Shimizu
H. Shimizu

References

1 Smith FJ, Jonkman MF, van Goor H *et al.* A mutation in human keratin K6b produces a phenocopy of the K17 disorder pachyonychia congenita type 2. *Hum Mol Genet* 1998; **7**:1143–8.
2 Terrinoni A, Smith FJ, Didona B *et al.* Novel and recurrent mutations in the genes encoding keratins K6a, K16 and K17 in 13 cases of pachyonychia congenita. *J Invest Dermatol* 2001; **117**:1391–6.
3 McLean WH, Smith FJ, Cassidy AJ. Insights into genotype–phenotype correlation in pachyonychia congenita from the human intermediate filament mutation database. *J Investig Dermatol Symp Proc* 2005; **10**:31–6.
4 Leachman SA, Kaspar RL, Fleckman P *et al.* Clinical and pathological features of pachyonychia congenita. *J Investig Dermatol Symp Proc* 2005; **10**:3–17.
5 McLean WH, Rugg EL, Lunny DP *et al.* Keratin 16 and keratin 17 mutations cause pachyonychia congenita. *Nat Genet* 1995; **9**:273–8.
6 Smith FJ, Liao H, Cassidy AJ *et al.* The genetic basis of pachyonychia congenita. *J Investig Dermatol Symp Proc* 2005; **10**:21–30.
7 Wu JW, Xiao SX, Liu Y *et al.* Identification of two recurrent mutations in keratin genes in three cases with pachyonychia congenita. *J Eur Acad Dermatol Venereol* 2008 Apr 22 [Epub ahead of print].

Key words: *autosomal dominant disorders, heterodimer, intermediate filament, keratin disease, pilosebaceous cysts*

Conflicts of interest: none declared.

Metastatic prostate cancer presenting as paraneoplastic pemphigus: a favourable clinical response to combined androgen blockade and conventional immunosuppressive therapy

DOI: 10.1111/j.1365-2133.2008.08982.x

Sir, Paraneoplastic pemphigus (PNP), first described in 1990, is an autoimmune mucocutaneous blistering disease which is associated with an underlying malignancy and is characterized by polymorphic clinical signs.[1] Pathogenesis is due to an aberrant autoimmune response against the proteins of the plakin family such as plectin, envoplakin, periplakin, desmoplakin I and II, and bullous pemphigoid antigen I (BP230),[2] although several cases of PNP with antibodies to desmoglein (Dsg) 1 and 3 have been described.[3]

A 77-year-old man was admitted to our Oral Medicine Unit because of recalcitrant severe oral bullous/erosive mucositis with crusting lesions of the lips (Fig. 1a), accompanied by marked conjunctivitis of both eyes (Fig. 1b), with cutaneous bullous lesions of the abdomen and bilaterally of the hip and inguinal area (Fig. 1c). Nikolsky's sign, performed on the oral mucosa and skin, was positive.

Oral biopsy revealed suprabasal epithelial detachment with an eosinophilic and neutrophilic infiltrate. Direct immunofluorescence showed positive fluorescence in the intercellular cement substance (ICS) of IgG and complement 3c, while IgA and IgM were negative. Indirect immunofluorescence, using normal human skin as substrate, showed an intercellular signal confined to the ICS with a titre of 1 : 360. Enzyme-linked immunosorbent assay gave a value of 54 U mL^{-1} for Dsg1 (normal 0–14) and a value of 162 U mL^{-1} for Dsg3 (normal 0–14), confirming a diagnosis of pemphigus vulgaris.

PNP was suspected due to the severe and polymorphic mucocutaneous involvement, in particular of the conjunctiva and labial mucosa, which resembled erythema multiforme-like lesions. Routine haematological tests, serum tumour markers [β_2-microglobulin, prostate-specific antigen (PSA), alpha-fetoprotein, carcinoembryonic antigen, Ca 19-9, Ca 72-4, Ca 125, acid phosphatase, Bence-Jones proteinuria], chest X-ray, echocardiogram, colonoscopy and oesophagogastroduodenoscopy were negative except for microhaematuria and an elevated level of PSA (49·1 ng mL^{-1}; normal 0–4). A total body computed tomography (CT) scan revealed enlargement of the prostate, while bone scintigraphy revealed multiple foci of increased uptake (L2–L3, D8–D10). An ultrasound-guided needle biopsy of the prostate revealed a diffuse infiltration of adenocarcinoma. The prostate cancer grading (Gleason scale) was 8 (4 + 4). Immunoblotting analysis revealed the presence of antibodies to 250-, 210-, 190-, 160- and 130-kDa proteins (Fig. 2). So, in line with the criteria previously proposed,[2] a diagnosis of PNP was confirmed. Investigations by an internist and an otorhinolaryngologist were negative. High-resolution CT scan and tests for pulmonary function ruled out bronchiolitis obliterans.

The patient received conventional immunosuppressive therapy (CIST) comprising prednisone 100 mg daily and azathioprine 150 mg daily, and, at the same time, was referred to a nearby urological unit where he received combined androgen blockade (CAB) therapy comprising bicalutamide 150 mg and tamsulosin chlorohydrate 0·4 mg daily, goserelin acetate 10·8 mg every 75 days, alendronic acid 70 mg once weekly, and calcium carbonate/cholecalciferol 500 mg/440 IU every other day.

After 6 months, he was in complete clinical (Fig. 1d–f) and immunological remission on therapy (prednisone 50 mg twice weekly and azathioprine 50 mg daily), although still taking CAB, alendronic acid and calcium carbonate/cholecalciferol. The PSA level was 0·446 ng mL^{-1} and bone scintigraphy revealed only two foci with weak hypercaptation (areas of increased uptake).

It has been postulated that the autoimmune response in PNP may be twofold: (i) humoral, via cross-reaction of foreign tumour antigens to epidermal antigens, or production of plakin proteins induced by the tumour, or an epitope spreading phenomenon,[4] and (ii) cell mediated, via activation of CD8+ cytotoxic T lymphocytes, CD56+ natural killer

Uncorrected Version. Published on November 5, 2009 as DOI:10.2353/ajpath.2009.090347

The American Journal of Pathology, Vol. 175, No. 6, December 2009

DOI: 10.2353/ajpath.2009.090347

Molecular Pathogenesis of Genetic and Inherited Diseases

Keratinocyte-/Fibroblast-Targeted Rescue of *Col7a1*-Disrupted Mice and Generation of an Exact Dystrophic Epidermolysis Bullosa Model Using a Human *COL7A1* Mutation

Kei Ito,* Daisuke Sawamura,* Maki Goto,* Hideki Nakamura,* Wataru Nishie,* Kaori Sakai,* Ken Natsuga,* Satoru Shinkuma,* Akihiko Shibaki,* Jouni Uitto,† Christopher P. Denton,‡ Osamu Nakajima,§ Masashi Akiyama,* and Hiroshi Shimizu*

From the Department of Dermatology, Hokkaido University Graduate School of Medicine, Sapporo, Japan; Department of Dermatology and Cutaneous Biology,† Jefferson Medical College and Jefferson Institute of Molecular Medicine, Thomas Jefferson University, Philadelphia, Pennsylvania; Department of Medicine,‡ Royal Free Campus, University College London, London, United Kingdom; and Research Laboratory for Molecular Genetics,§ Yamagata University, Yamagata, Japan*

Recessive dystrophic epidermolysis bullosa (RDEB) is a severe hereditary bullous disease caused by mutations in *COL7A1*, which encodes type VII collagen (COL7). *Col7a1* knockout mice ($COL7^{m-/-}$) exhibit a severe RDEB phenotype and die within a few days after birth. Toward developing novel approaches for treating patients with RDEB, we attempted to rescue $COL7^{m-/-}$ mice by introducing human *COL7A1* cDNA. We first generated transgenic mice that express human *COL7A1* cDNA specifically in either epidermal keratinocytes or dermal fibroblasts. We then performed transgenic rescue experiments by crossing these transgenic mice with $COL7^{m+/-}$ heterozygous mice. Surprisingly, human COL7 expressed by keratinocytes or by fibroblasts was able to rescue all of the abnormal phenotypic manifestations of the $COL7^{m-/-}$ mice, indicating that fibroblasts as well as keratinocytes are potential targets for RDEB gene therapy. Furthermore, we generated transgenic mice with a premature termination codon expressing truncated COL7 protein and performed the same rescue experiments. Notably, the $COL7^{m-/-}$ mice rescued with the human *COL7A1* allele were able to survive despite demonstrating clinical manifestations very similar to those of human RDEB, indicating that we were able to generate surviving animal models of RDEB with a mutated human *COL7A1* gene. This model has great potential for future research into the pathomechanisms of dystrophic epidermolysis bullosa and the development of gene therapies for patients with dystrophic epidermolysis bullosa. *(Am J Pathol 2009, 175:000–000; DOI: 10.2353/ajpath.2009.090347)*

Dystrophic epidermolysis bullosa (DEB) is clinically characterized by mucocutaneous blistering in response to minor trauma, followed by scarring and nail dystrophy. The blistering occurs along the epidermal basement membrane zone (BMZ) just beneath the lamina densa at the level of the anchoring fibrils. The inheritance of DEB can be autosomal dominant (DDEB) or autosomal recessive (RDEB), each comprising subtypes of different clinical presentations and severities.[1] Both DDEB and RDEB are known to be caused by mutations in the *COL7A1* gene encoding type VII collagen (COL7), the major component of anchoring fibrils.[2] The most severe RDEB subtype, the Hallopeau-Siemens subtype, shows a complete lack of expression of type VII collagen, whereas a less severe RDEB subtype, the non-Hallopeau-Siemens subtype, shows some collagen expression. The clinical fea-

Supported in part by a Grant-in-Aid for Scientific Research from the Japanese Society for the Promotion of Science, by a grant from Ministry of Health, Labour and Welfare of Japan (Health and Labour Sciences Research Grants; Research on Intractable Diseases) and by the National Institute of Arthritis & Musculoskeletal & Skin Diseases, National Institutes of Health (grant R01-AR54876-01).

K.I. and D.S. contributed equally to this work.

Accepted for publication August 20, 2009.

A guest editor acted as editor-in-chief for this manuscript. No person at Thomas Jefferson University was involved in the peer review process or final disposition for this article.

Address reprint requests to Hiroshi Shimizu M.D., Ph.D., Department of Dermatology, Hokkaido University Graduate School of Medicine, N15 W7, Kita-ku, Sapporo 060-8638, Japan. E-mail: shimizu@med.hokudai.ac.jp

tures of DDEB are, in general, milder than those of RDEB and tend to improve with age. The molecular mechanisms of DEB have been thoroughly investigated, and precise diagnosis and estimation of prognosis is now possible. There is no specific treatment for different forms of DEB, and the current focus of research is to develop more effective treatments for this group of blistering disorders.

Corrective gene therapy whereby normal COL7 is introduced into the patients' cells, has great potential as a treatment for DEB. However, several obstacles must be overcome before its clinical therapeutic application. First, there have been no useful DEB animal models that reproduce the human mutated gene for experiments. Although COL7 knockout mice have been generated, most of such mice die within a few days of birth, and none survive more than 2 weeks.[3] A surviving DEB mouse that was reported recently was the DEB hypomorphic mouse model.[4] These mice, which had about 10% of the normal mouse COL7, did not show the abnormal form and function of anchoring fibrils seen in human patients of RDEB. Second, no studies have examined in detail whether the introduction of the human COL7 gene into DEB mouse cells can rescue the DEB phenotype without causing adverse effects in a living DEB model. Third, there is controversy over which cells may serve as optimal targets in gene therapies for DEB. Several studies have targeted keratinocytes, because the cells that secrete COL7 are mainly keratinocytes and to a lesser extent fibroblasts.[5,6] However, we and others have recently reported that injection of gene-transferred fibroblasts into the skin can efficiently restore COL7 expression in the dermal-epidermal junction *in vitro*.[6–8] Furthermore, intradermal injection of allogeneic fibroblasts into skin of patients with RDEB skin was shown to result in enhanced COL7 expression in selected patients.[9] Therefore, we need to compare keratinocytes and fibroblasts to clarify their efficacy as target cells in an *in vivo* model system of RDEB.

To address these issues, we generated transgenic mice with human *COL7A1* under different promoters and performed transgenic rescue experiments on the Col7a1$^{m-/-}$ background using those transgenic mice. Furthermore, to develop a DEB model that accurately reproduces human DEB not only in terms of clinical manifestations but also in terms of gene mutation, we also introduced a mutated human *COL7A1* gene into this mouse model system and created human mutant gene-expressing rescued mice corresponding to the surviving animal of DEB. Our results advance our understanding of the function and biology of COL7.

Materials and Methods

Generation of Transgenic Mice

Human full-length *COL7A1* cDNA was constructed from several overlapping cDNA clones (Sawamura et al, 2002). We used a pCMVβ expression vector (Invitrogen, Carlsbad, CA) that contained the cytomegalovirus (CMV) promoter, the simian virus 40 (SV40) splice donor/splice acceptor site, the *lacZ* gene, and the SV40 polyadenylation signal. We selected human keratin 14 (K14),[10] the mouse pro-α 2 chain of type I collagen (col1a2),[11] or the CMV promoter for epidermis-specific, dermis-specific, or ubiquitous expression of the transgene, respectively. We first modified pCMVβ by replacing LacZ with human full-length *COL7A1* cDNA, and the CMV promoter with the human K14 or the mouse col1a2 gene. Finally, we produced three *COL7A1* constructs for transgenic mice (Figure 1A). They were digested with appropriate restriction enzymes, purified, and introduced into BDF1 oocytes, which were subsequently transplanted into the recipient mice. Founders were bred to wild-type C57BL/6 females. To confirm germline transmission, PCR analyses on genomic DNA were performed (forward, 5′-CTCAGTGGATGTTGCCTTT-3′; reverse, 5′-TAAGAACACAATGTCAGCGG-3′) using specific primers and the following thermal cycling parameters: 94°C for 5 minutes, 94°C for 45 seconds, and 56°C for 45 seconds; followed by 35 cycles at 72°C for 45 seconds and 72°C for 7 minutes. The transgenic (Tg) mice with K14, col1a2, and CMV

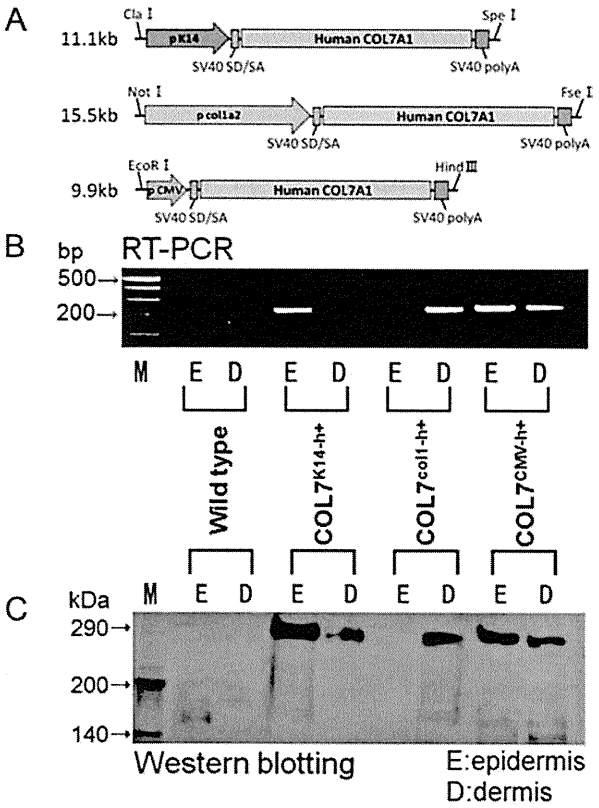

Figure 1. Epidermis- or dermis-specific expression of the human *COL7A1* full-length cDNA in the transgenic mice. **A:** Three expression vectors for transgenic mice were constructed using the promoters of human K14, mouse col1a2, and CMV. The vector contains the SV40 splice donor/splice acceptor (SD/SA) site and the SV40 polyadenylation (polyA) signal. **B:** We obtained epidermis and dermis from the K14Tg mice (COL7$^{K14\text{-}h+}$), col1a2Tg mice (COL7$^{col1\text{-}h+}$), and CMVTg mice (COL7$^{CMV\text{-}h+}$) and then examined human *COL7A1* mRNA expression by RT-PCR analysis. Molecular weight markers (M) are a 100-bp DNA ladder. **C:** Expression of COL7 was also investigated by Western blot analysis using anti-human monoclonal antibody LH7.2. Molecular weight markers are a biotinylated protein ladder.

Table 1. Summary of the Genetically Engineered Mice Involved in This Study

Mouse	Genotype	Phenotype
$COL7^{m-/-}$	Knockout mouse with targeted disruption of the mouse *Col7a1* encoding mouse type VII collagen	RDEB (severe disease phenotype)
$COL7^{m+/-}$	*Col7a1* heterozygous knockout mouse	Clinically normal
$COL7^{K14\text{-}h+}$	Transgenic mouse with human *COL7A1* driven by the human K14 promoter	Clinically normal
$COL7^{col1\text{-}h+}$	Transgenic mouse with human *COL7A1* driven by the promoter of the gene encoding mouse pro-α 2 chain of type I collagen	Clinically normal
$COL7^{CMV\text{-}h+}$	Transgenic mouse with human *COL7A1* driven by the ubiquitous CMV promoter	Clinically normal
$COL7^{m-/-,\ K14\text{-}h+}$	*Col7a1* knockout mouse rescued by human *COL7A1* with the human K14 promoter	Clinically normal
$COL7^{m-/-,\ col1\text{-}h+}$	*Col7a1* knockout mouse rescued by human *COL7A1* with the mouse pro-α 2 chain of type I collagen promoter	Clinically normal
$COL7^{m-/-,\ CMV\text{-}h+}$	*Col7a1* knockout mouse rescued by human *COL7A1* with the CMV promoter	Clinically normal
$COL7^{K14\text{-}\Delta h+}$	Transgenic mouse with mutated human type VII collagen with 7528delG mutation under the human K14 promoter	Clinically normal
$COL7^{m-/-,\ K14\text{-}\Delta h+}$	*Col7a1* knockout mouse with the mutated human type VII collagen with 7528delG	RDEB (moderate disease phenotype)

promoters were designated as K14Tg mice ($COL7^{K14\text{-}h+}$), col1a2Tg mice ($COL7^{col1\text{-}h+}$), and CMVTg mice ($COL7^{CMV\text{-}h+}$), respectively (Table 1).

Transgenic Rescue Experiment

Transgenic mice with different promoters ($COL7^{K14\text{-}h+}$, $COL7^{col1\text{-}h+}$, and $COL7^{CMV\text{-}h+}$) were crossbred to heterozygous *col7a1* knockout mouse ($COL7^{m+/-}$) generated by Heinonen et al[3] to create heterozygous mice carrying human *COL7A1* cDNA. Then these mice were mated again with $COL7^{m+/-}$ mice to obtain a mouse that harbored the human COL7 gene in a *col7a1* knockout background. The resulting transgenic rescue mice, each with either the K14, col1a2, or CMV promoter, were, respectively, designated as $COL7^{m-/-,\ K14\text{-}h+}$, $COL7^{m-/-,\ col1\text{-}h+}$, and $COL7^{m-/-,\ CMV\text{-}h+}$ (Table 1). The rescued mice ($COL7^{m-/-,\ K14\text{-}h+}$, $COL7^{m-/-,\ col1\text{-}h+}$, and $COL7^{m-/-,\ CMV\text{-}h+}$) were analyzed by histopathological, immunofluorescence, and immunoblot analyses as described below. Whole-skin samples from the rescued mice were used for the immunoblot analysis.

RT-PCR and Western Blot Analysis

Mouse skin was obtained from the back of each mouse and incubated with 10 mg/ml dispase for 8 hours at 4°C to separate the epidermis and dermis. The epidermal and dermal sheets were minced, and total RNA was extracted using an RNeasy RNA extraction kit (Qiagen, Hilden, Germany). The cDNA was synthesized with the SuperScript First-Strand Synthesis System for RT-PCR (Invitrogen, Grand Island, NY) and subjected to PCR, using specific primers (forward, 5′-CTCAGTGGATGTTGCCTTTA-3′; reverse, 5′-TAAGAACACAATGTCAGCGG-3′) and the following thermal cycling parameters: 94°C for 5 minutes, 94°C for 1 minute, and 56°C for 1 minute; followed by 35 cycles at 72°C for 1 minute and 72°C for 7 minutes.

For Western blot analysis, the epidermal and dermal sheets were mixed with a protease inhibitor cocktail (Sigma-Aldrich, St. Louis, MO), homogenized, and centrifuged at 15,000 × *g*. The supernatant of each sample was separated on a 5% polyacrylamide gel under reducing conditions. Immunoblotting analysis was performed by incubation with the LH7.2 monoclonal antibody (1:1000) for 18 hours at 4°C and then with secondary goat anti-mouse IgG antibodies conjugated with peroxidase (1:2000) for 1 hour at 37°C. The resultant complexes were processed using the Phototope HRP Western Blot Detection System (Cell Signaling Technology, Beverly, MA) according to the manufacturer's protocol.

Histopathological, Immunofluorescence, Ultrastructural, and Immunoelectron Microscopic Analyses

Mouse skin samples were fixed in 10% formalin neutral buffer solution for paraffin embedding or were immediately frozen in OCT compound and stored at −80°C. Paraffin-embedded sections were cut to 5 μm and stained with H&E solution. Alternatively, the LH7.2 monoclonal antibody against the NC-1 amino-terminal domain of COL7 (Chemicon, Temecula, CA) was used for immunofluorescence staining on frozen sections from tissue samples embedded in OCT compound. The bound antibodies were detected with fluorescein isothiocyanate-conjugated goat anti-mouse IgG antibody (Jackson ImmunoResearch Laboratories, Inc., West Grove, PA). Nuclear counterstaining with propidium iodide was performed in some immunofluorescence labeling experiments.

For electron microscopic examination, skin specimens were fixed in 5% glutaraldehyde, postfixed in 1% osmium tetroxide, and stained en block in uranyl acetate. They were dehydrated in a graded ethanol series and embedded in Araldite 6005. Ultrathin sections were cut and stained with uranyl acetate and lead citrate. The sections were examined with a transmission electron microscope (H-7100; Hitachi, Tokyo, Japan) at 75 kV. For semiquantitative morphometric analysis, the number of anchoring fibrils on electron micrographs was counted and the number of anchoring fibrils per unit length of lamina

densa was estimated as number of anchoring fibrils/1 μm of lamina densa. Minimal anchoring fibril features required for quantification were the presence of an arch structure of fibrils inserted into the dermis from the lamina densa. Twenty electron microscopic sections were examined for each mouse line. For immunoelectron microscopic analysis, skin samples were cryofixed with liquid propane cooled with nitrogen, cryosubstituted at −80°C, and low temperature-embedded at −60°C in Lowicryl K11M resin before undergoing UV polymerization. Ultrathin sections were cut to 90 nm thickness. The LH7.2 monoclonal antibody was used as the primary antibody, and then a goat anti-rabbit IgG 10-nm gold-conjugated secondary antibody was used (Amersham, Poole, UK). The sections were stained with uranyl acetate and lead citrate and examined with a transmission electron microscope.

Transgenic Rescue Experiment with the Human Mutated Gene

We generated a full-length human *COL7A1* cDNA containing the c.7528delG mutation and replaced the normal human *COL7A1* cDNA K14 promoter construct (Figure 1A) with the human mutated *COL7A1* cDNA (c.7528delG). The guanine at 7528 is at the end of the collagenous domain of COL7, and the mutation creates a premature stop codon at 18 bp downstream. The expressed protein is a truncated COL7 lacking the NC-2 domain at the C terminus. Using the same techniques as described above, we produced transgenic mice by microinjection, screening PCR, and germline transmission. The transgenic mice ($COL7^{K14\text{-}\Delta h+}$) were crossbred to heterozygous *col7a1* knockout mouse ($COL7^{m-/-}$). Then these mice ($COL7^{m+/-,\ K14\text{-}\Delta h+}$) were intercrossed to obtain a mouse that harbored the mutated human COL7 gene in a *col7a1* knockout background (Table 1). The rescued mice ($COL7^{m-/-,\ K14\text{-}\Delta h+}$) were analyzed by histopathological, immunofluorescence, and immunoblot analyses as described above.

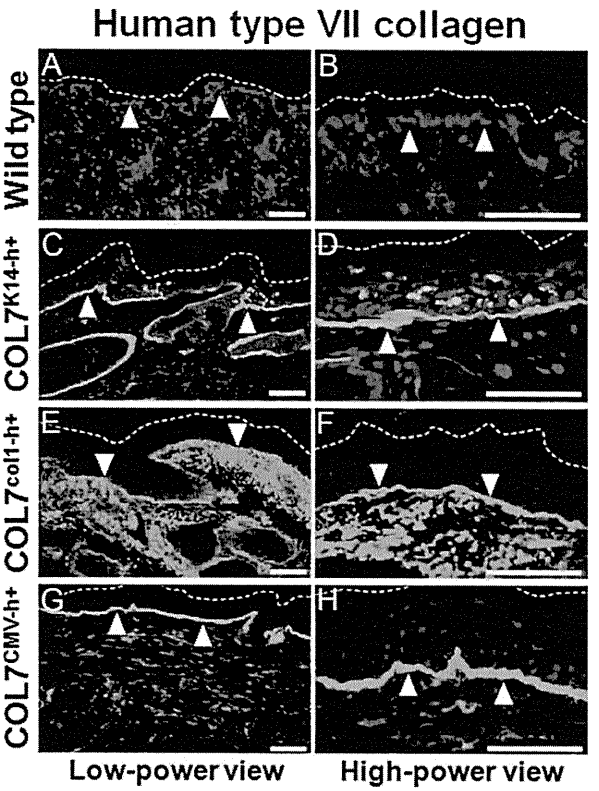

Figure 2. Both epidermis- and dermis-targeted transgene products of human COL7 molecules were precisely localized in the dermoepidermal junction in the transgenic mice. Immunofluorescence staining with the anti-human COL7 monoclonal antibody LH7.2 showed no human COL7 immunolabeling in the dermoepidermal junction of the wild-type mouse skin (**A** and **B**). Skin samples from all three transgenic mouse lines (keratinocyte-targeted K14Tg mice ($COL7^{K14\text{-}h+}$) (**C** and **D**), fibroblast-targeted col1a2Tg mice ($COL7^{col1\text{-}h+}$) (**E** and **F**), and CMVTg mice with ubiquitous COL7 expression ($COL7^{CMV\text{-}h+}$) (**G** and **H**) showed human COL7 linear staining at the epidermal BMZ (**white arrowheads**). $COL7^{K14\text{-}h+}$ mouse skin revealed additional punctate staining in epidermal keratinocytes, and $COL7^{col1\text{-}h+}$ mouse skin showed additional diffuse staining in dermal fibroblasts. Dotted lines demarcate the skin surface. Left column (**A, C, E,** and **G**), low-power view; right column (**B, D, F,** and **H**), high-power view. Human COL7 immunolabeling, green (fluorescein isothiocyanate); nuclear stain, red (propidium iodide). Scale bars = 50 μm.

Results

Generation of Transgenic Mice Showing Keratinocyte- or Fibroblast-Targeted Expression of Human COL7

To allow selective expression of human *COL7A1* in epidermal keratinocytes or in dermal fibroblasts, we used human K14 and mouse col1a2 promoters, which have been shown to specify epidermal and dermal expression in mice, respectively.[10,11] The mice with K14 or col1a2 promoters were designated as K14Tg mice ($COL7^{K14\text{-}h+}$) and col1a2Tg mice ($COL7^{col1\text{-}h+}$), respectively (Figure 1A). In addition, the ubiquitous CMV promoter was used to generate transgenic mice with both epidermal and dermal expression (CMVTg mice: $COL7^{CMV\text{-}h+}$) (Figure 1A). To demonstrate tissue-specific expression, we obtained epidermis and dermis from the mice and determined *COL7A1* mRNA expression by RT-PCR analysis using primers specific for human transcripts. The results show that $COL7^{K14\text{-}h+}$ mice *COL7A1* mRNA expression is restricted to the epidermis and mRNA expression of *COL7A1* in $COL7^{col1\text{-}h+}$ mice is restricted to the dermis. Expression of epidermal and dermal *COL7A1* mRNA was detected in $COL7^{CMV\text{-}h+}$ mice (Figure 1B). Western blot analysis also shows epidermal or dermal expression mostly consistent with the specific promoters, except for a weak COL7 band detected in the dermal component from $COL7^{K14\text{-}h+}$ mice (Figure 1C). A small amount of COL7 secreted by epidermal keratinocytes moves into the dermal side. The weak COL7 band in the dermal component from $COL7^{K14\text{-}h+}$ mice probably reflects the translocated COL7 peptides.

Immunofluorescence study using LH7.2 anti-human COL7 monoclonal antibody showed the linear epidermal

BMZ staining in all three transgenic mice lines (Figure 2, A and B, wild-type; Figure 2, C and D, $COL7^{K14\text{-}h+}$; Figure 2, E and F, $COL7^{col1\text{-}h+}$; and Figure 2, G and H, $COL7^{CMV\text{-}h+}$). $COL7^{K14\text{-}h+}$ revealed additional punctate staining in epidermal keratinocytes (Figure 2, C and D), and $COL7^{col1\text{-}h+}$ revealed additional diffuse staining in dermal fibroblasts (Figure 2, E and F). In the course of the transgenic mouse experiments, we obtained several lines of mice and were able to generate offspring in $COL7^{K14\text{-}h+}$, $COL7^{col1\text{-}h+}$, and $COL7^{CMV\text{-}h+}$ lineages. In each transgenic line, we selected the mouse with the most robust *COL7A1* expression for the subsequent rescue experiments.

Keratinocyte-/Fibroblast-Targeted Transgenic Rescue of COL7 Knockout Mice

Col7a1 knockout mice ($COL7^{m-/-}$) exhibit a severe, recessive DEB phenotype, and these mice die within a few days after birth. We initiated transgenic rescue experiments of $COL7^{m-/-}$ mice by mating $COL7^{m+/-}$, $COL7^{col1\text{-}h+}$, or $COL7^{CMV\text{-}h+}$ transgenic mice. After further crossing, transgenic mice on a *col7a1* knockout background ($COL7^{m-/-,\ K14\text{-}h+}$, $COL7^{m-/-,\ col1\text{-}h+}$, and $COL7^{m-/-,\ CMV\text{-}h+}$) were generated, and they showed expression of human COL7 under the different promoters. All three different rescued mice ($COL7^{m-/-,\ K14\text{-}h+}$,

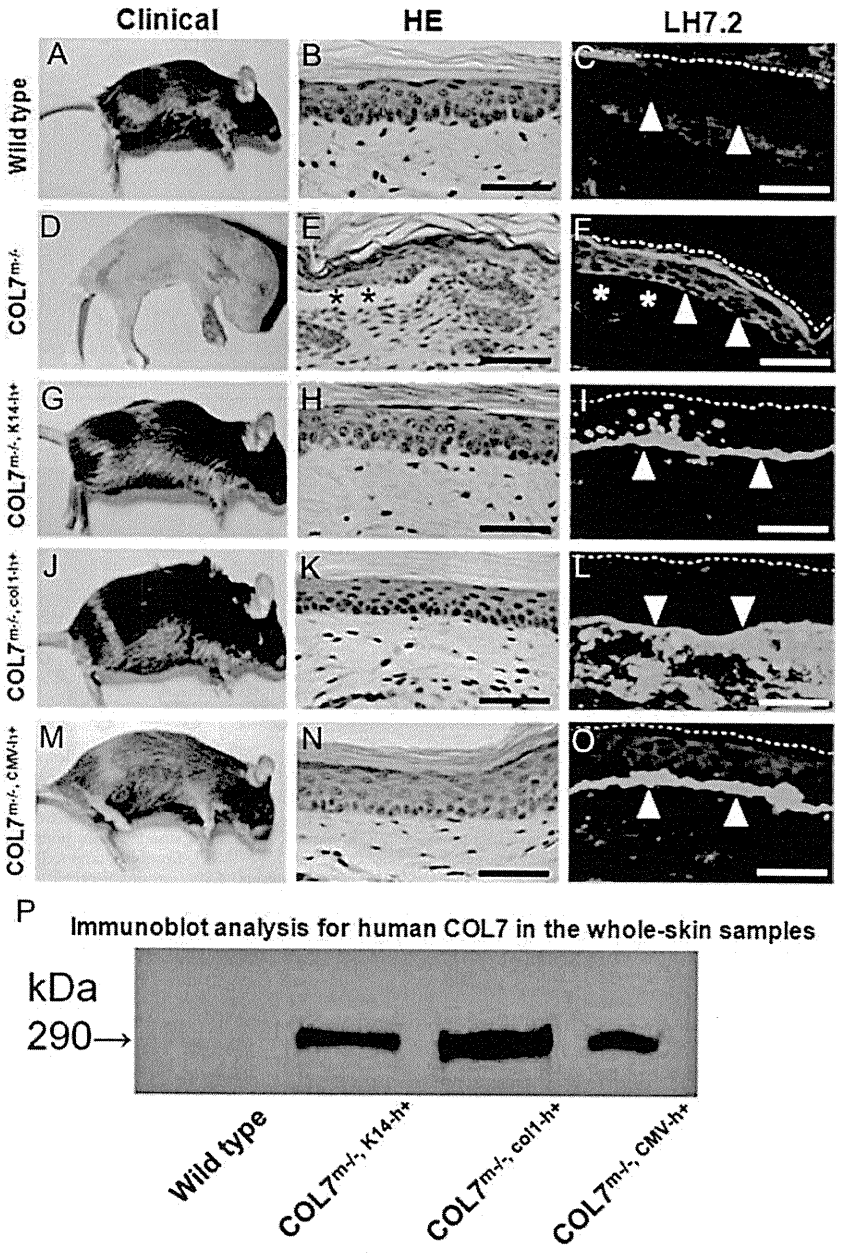

Figure 3. Keratinocyte-/fibroblast-targeted human *COL7A1* transgene can rescue COL7 knockout mice. A wild-type mouse showed a normal phenotype (**A**) and intact dermoepidermal junction (**B**) without human COL7 expression (**C, white arrowheads**). A $COL7^{m-/-}$ mouse had a severe DEB phenotype (**D**) and apparent dermoepidermal separation (**E, asterisks**) without human COL7 (**F, white arrowheads**). All three rescued mice (keratinocyte-targeted rescued $COL7^{m-/-,\ K14\text{-}h+}$ [**G–I**], fibroblast-targeted rescued $COL7^{m-/-,\ col1\text{-}h+}$ [**J–L**]), and ubiquitous CMV promoter-driven rescued $COL7^{m-/-,\ CMV\text{-}h+}$ [**M-O**]) showed no DEB phenotype (**G, J,** and **M**) and an intact dermoepidermal junction (**H, K,** and **N**). Immunofluorescence labeling revealed human COL7 in the basement membrane zone (**white arrowheads**) in skin sections from all three rescued mice (**I, L,** and **O**). Skin from the keratinocyte-targeted rescued $COL7^{m-/-,\ K14\text{-}h+}$ mouse showed additional punctate staining in epidermal keratinocytes (**I**), and skin from the fibroblast-targeted rescued $COL7^{m-/-,\ col1\text{-}h+}$ mouse revealed additional diffuse staining in dermal fibroblasts (**L**). Immunofluorescence staining with anti-human COL7 monoclonal antibody, LH7.2, fluorescein isothiocyanate, green (**C, F, I, L,** and **O**). **White arrowheads**, basement membrane zone; **asterisks,** a blister cavity. Dotted lines demarcate the skin surface. Scale bars = 50 μm. **P:** Immunoblot analysis for human COL7 in the whole-skin samples from the wild-type and the three rescued mouse lines. Human COL7 protein expression was confirmed in the whole skin of all three lines of rescued mice ($COL7^{m-/-,\ K14\text{-}h+}$, $COL7^{m-/-,\ col1\text{-}h+}$, and $COL7^{m-/-,\ CMV\text{-}h+}$) but not in the wild-type mice. From the density of immunoblot bands, amounts of human COL7 expressed in the whole-skin samples were the greatest in $COL7^{m-/-,\ col1\text{-}h+}$ line among the three lines of rescued mice. The other two rescued lines, $COL7^{m-/-,\ CMV\text{-}h+}$ and $COL7^{m-/-,\ K14\text{-}h+}$, expressed roughly similar amounts of human COL7.

$COL7^{m-/-,\ col1\text{-}h+}$, and $COL7^{m-/-,\ CMV\text{-}h+}$) showed normal appearance at birth, and no DEB phenotype was observed (Figure 3, A, D, G, J, and M). Remarkably, all of the rescued mice ($COL7^{m-/-,\ K14\ hours\text{-}+}$, $COL7^{m-/-,\ col1\text{-}h+}$, and $COL7^{m-/-,\ CMV\text{-}h+}$) exhibited reproductive ability despite the fact that the original $COL7^{m-/-}$ mice were lethal and unable to reproduce. All of these rescued mice had at least a 1-year lifespan, similar to that of wild-type mice. We could not detect any blistering, even on a histological scale (Figure 3, B, E, H, K, and N) and immunofluorescence study using LH7.2 showed positive linear staining of COL7 along the BMZ in all three lines of rescued mice ($COL7^{m-/-,\ K14\text{-}h+}$, $COL7^{m-/-,\ col1\text{-}h+}$, and $COL7^{m-/-,\ CMV\text{-}h+}$) (Figure 3, C, F, I, L, and O). The pattern of positive staining was essentially identical to that in the respective original transgenic mice (Figure 2, A–H). Immunoblot analysis for human COL7 in the whole-skin samples from the transgenic rescued mice confirmed that human COL7 protein was expressed in the whole skin of all three lines of rescued mice ($COL7^{m-/-,\ K14\text{-}h+}$, $COL7^{m-/-,\ col1\text{-}h+}$, and $COL7^{m-/-,\ CMV\text{-}h+}$) (Figure 3P). The thicknesses of the immunoblot bands suggested that, in the whole-skin samples, $COL7^{m-/-,\ col1\text{-}h+}$ expressed the most human COL7 among the three lines of rescued mice, and the other two rescued lines, $COL7^{m-/-,\ CMV\text{-}h+}$ and $COL7^{m-/-,\ K14\text{-}h+}$, produced similarly less human COL7.

Electron microscopy of the skin showed newly formed anchoring fibrils in the sublamina densa area in all of the rescued mice ($COL7^{m-/-,\ K14\text{-}h+}$, $COL7^{m-/-,\ col1\text{-}h+}$, and $COL7^{m-/-,\ CMV\text{-}h+}$) (Figure 4, A, C, E, G, and I). Semiquantitative morphometric analysis of numbers of anchoring fibrils on electron microscopic images revealed the anchoring fibril density in each mouse line as follows (mean ± SD number of anchoring fibrils/μm): wild-type $COL7^{m+/+}$, 3.41 ± 0.43; $COL7^{m-/-}$, 0.00 ± 0.00; $COL7^{m-/-,\ K14\text{-}h+}$, 2.60 ± 0.46; $COL7^{m-/-,\ col1\text{-}h+}$, 2.85 ± 0.39; and $COL7^{m-/-,\ CMV\text{-}h+}$, 3.09 ± 0.30 (Figure 4K). Immunoelectron microscopic analysis of the skin obtained from each line of rescued mice revealed that LH7.2-labeled gold particles were localized in the lamina densa of the BMZ (Figure 4, B, D, F, H, and J). The epitopes of LH7.2 monoclonal antibody are known to react to the NC-1 domain of COL7, which is known to be located along the lamina densa.[12] The results suggest that COL7 synthesized from transgenes functioned correctly, irrespective of whether it originated from fibroblasts or from keratinocytes.

Generation of an Exact DEB Model Mice Carrying Human COL7A1 Mutation

In the course of cloning experiments, we obtained several mutant *COL7A1* clones that demonstrated abnormal *COL7A1* expression. Subsequent sequence analysis revealed that one of those clones had a c.7528delG mutation in the *COL7A1* cDNA. We then constructed an expression vector of the mutated *COL7A1* under the K14 promoter and generated the transgenic mice. Next, we crossed these mutant $COL7^{K14\text{-}\Delta h+}$ transgenic mice with $COL7^{m+/-}$ het-

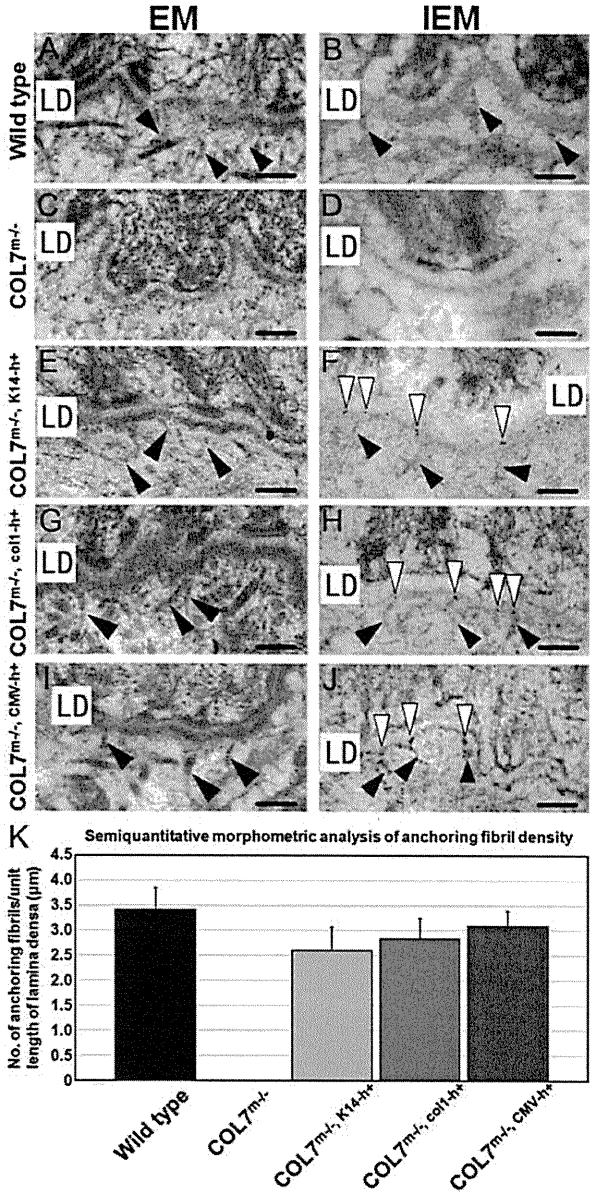

Figure 4. Transgene products, which are human COL7 molecules, correctly form anchoring fibrils in the rescued mice. Electron microscopy (EM) (**A, C, E, G,** and **I**) demonstrated intact anchoring fibrils (**black arrowheads**) in the sublamina densa area in a wild-type mouse (**A**). In contrast, the $COL7^{m-/-}$ mouse had no anchoring fibrils (**C**). In all three rescued mice lines (keratinocyte-targeted rescued $COL7^{m-/-,\ K14\text{-}h+}$ [**E**], fibroblast-targeted rescued $COL7^{m-/-,\ col1\text{-}h+}$ [**G**], and ubiquitous CMV promoter-driven rescued $COL7^{m-/-,\ CMV\text{-}h+}$ [**I**]), anchoring fibril formation was restored in the sublamina densa area (**black arrowheads**). Immunoelectron microscopy (IEM) using LH7.2 (**B, D, F, H,** and **J**) revealed no human COL7 labeling (gold particle) in intact anchoring fibrils (**black arrowheads**) of a wild-type mouse (**B**). The $COL7^{m-/-}$ mouse had neither anchoring fibrils nor human COL7 labeling (**D**). Human COL7 (immunogold particles, **white arrowheads**) was localized in the lamina densa of the basement membrane zone in all three rescued mice: keratinocyte-targeted rescued $COL7^{m-/-,\ K14\text{-}h+}$ (**F**), fibroblast-targeted rescued $COL7^{m-/-,\ col1\text{-}h+}$ (**H**), and ubiquitous CMV promoter-driven rescued $COL7^{m-/-,\ CMV\text{-}h+}$ (**J**). **Black arrowheads**, anchoring fibrils; **white arrowheads**, human COL7 labeling (immunogold particles); LD, lamina densa. Scale bars = 200 nm. **K:** Semiquantitative morphometric analysis of anchoring fibril density. Anchoring fibril density was highest in ubiquitous CMV promoter-driven rescued $COL7^{m-/-,\ CMV\text{-}h+}$, second highest in fibroblast-targeted rescued $COL7^{m-/-,\ col1\text{-}h+}$, and lowest in keratinocyte-targeted rescued $COL7^{m-/-,\ K14\text{-}h+}$ mice, among the three lines of rescued mice, although no statistically significant difference was observed between any combination of the three lines.

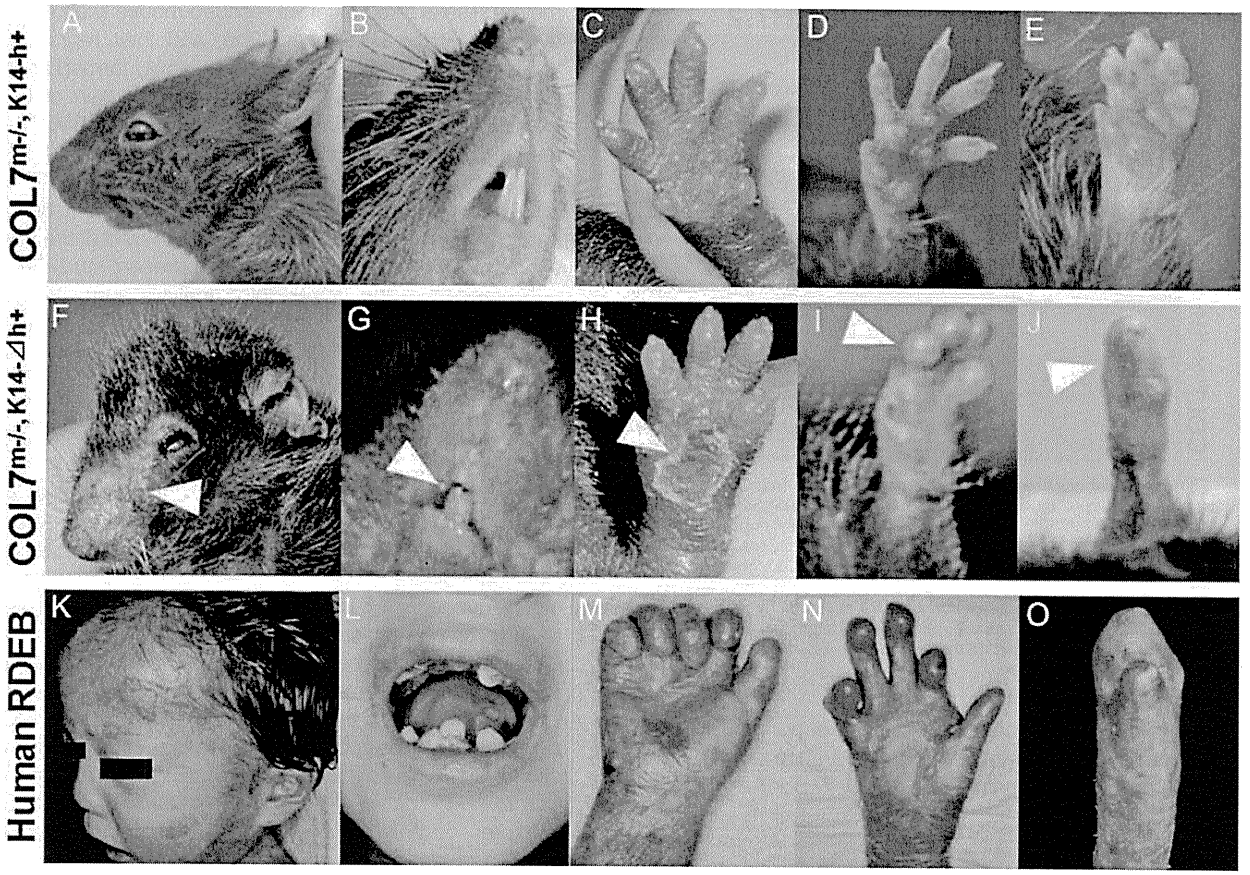

Figure 5. DEB model mice carrying a human *COL7A1* mutation precisely reproduce the DEB phenotype. **A–E:** *Col7a1* knockout mice rescued by full-length human *COL7A1* ($COL7^{m-/-, K14\text{-}h+}$) are clinically normal. Forepaws of $COL7^{m-/-, K14\text{-}h+}$ mice at 14 days (**C**), 30 days (**D**), and 60 days of age (**E**). **F–J:** *Col7a1* knockout mice rescued by mutated human *COL7A1* ($COL7^{m-/-, K14\text{-}\Delta h+}$) show gradual development of mild alopecia (**F**), yellowish dental caries (**G**), and fusion of the paw digits (**I** and **J**), corresponding to the clinical phenotype of human DEB. (**K** and **M:** A 2-year-old male patient harboring *COL7A1* mutations, c.[5818delC] + p.[Gly2623Ser].[13] **L:** A 10-year-old female patient whose mutations were unidentified. The diagnosis was confirmed by ultrastructural observation and immunofluorescence studies. **N:** A 15-year-old male patient with p.[Gly2576Arg] + [Glu2858X].[14] **O:** A 51-year-old female patient harboring p.[Gly1815Arg] + c.[5818delC].[15]) Forepaws of $COL7^{m-/-, K14\text{-}\Delta h+}$ mice were documented at 14 days (**H,** scarring), 30 days (**I,** mild fusion), and 60 days of age (**J,** complete fusion) (**white arrowheads**).

erozygous mice to obtain mutant $COL7^{m+/-, K14\text{-}\Delta h+}$ mice. We then performed transgenic rescue experiments by intercrossing these mice ($COL7^{m+/-, K14\text{-}\Delta h+}$) and obtained $COL7^{m-/-, K14\text{-}\Delta h+}$ mice. Immunoblot analysis on epidermal extract samples from $COL7^{m-/-, K14\text{-}\Delta h+}$ mice confirmed the expression of short, truncated human COL7 derived from mutant COL7A1 (data not shown).

From birth, the $COL7^{m-/-, K14\text{-}\Delta h+}$ mice were indistinguishable from their wild-type littermates and showed no blistering, not even on the paws, despite the fact that hemorrhagic bullae are always found in $COL7^{m-/-}$ mice. The growth of the human mutant-rescued mice ($COL7^{m-/-, K14\text{-}\Delta h+}$) was retarded, however, compared with that of their wild-type littermates. Interestingly, the $COL7^{m-/-, K14\text{-}\Delta h+}$ mice gradually developed the DEB phenotype, including nail dystrophy, scarring on the paws, fusion of the digits, yellowish dental caries, and mild alopecia, characteristic features of human RDEB (Figure 5, K–O).[13–15] It was difficult to distinguish the alopecia seen in the $COL7^{m-/-, K14\text{-}\Delta h+}$ mice from barbarism only from clinical appearance. However, the penetration of the alopecia is almost 100% in the $COL7^{m-/-, K14\text{-}\Delta h+}$ mice, whereas only a few wild-type littermates that were kept in the same condition showed barbarism. Thus, this alopecia was considered to be a feature specific to the $COL7^{m-/-, K14\text{-}\Delta h+}$ mice. These DEB clinical phenotypic manifestations were evident at 2 months of age (Figure 5, F–J). The clinical course of the forepaws showed a phenotype that is very characteristic of DEB. The $COL7^{m-/-, K14\text{-}\Delta h+}$ mice showed no blistering at birth, yet there was scarring of the forepaws 2 weeks later (Figure 5H). By 1 month, the paws had become mildly fused (Figure 5I), and complete fusion of paws (mitten deformity) was observed at 2 months (Figure 5J). The growth of the full-length human gene-rescued mice ($COL7^{m-/-, K14\text{-}h+}$) did not differ notably from that of the wild-type mice (Figure 5, A–E). During histopathological investigation, although clinically detectable blistering was not observed, we demonstrated microblistering along the dermal-epidermal junction in these mice ($COL7^{m-/-, K14\text{-}\Delta h+}$) by histopathological analysis (Figure 6, A and C). Immunofluorescence analysis showed immunoreactivity of human COL7 in the BMZ of the $COL7^{m-/-, K14\text{-}\Delta h+}$ mice (Figure 6, B and D). Most of the human mutant mice had about a 6-month lifespan (Figure 5,

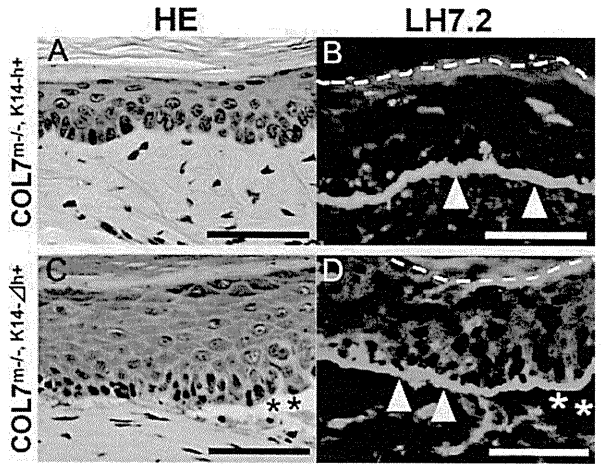

Figure 6. The humanized DEB model mouse shows subepidermal blistering with deposition of mutant human COL7 at the dermoepidermal junction. **A:** A $COL7^{m-/-,\ K14\text{-}h+}$ mouse has histopathologically normal skin. **C:** A $COL7^{m-/-,\ K14\text{-}\Delta h+}$ mouse shows subepidermal blistering (**asterisks**). **B** and **D:** Immunofluorescence study using anti-human COL7 antibody, LH7.2, reveals positive linear staining within the BMZ (**white arrowheads**), corresponding to normal and mutant human COL7 in a $COL7^{m-/-,\ K14\text{-}h+}$ mouse and a $COL7^{m-/-,\ K14\text{-}\Delta h+}$ mouse, respectively (**asterisks** indicate a blister cavity). Dotted lines demarcate the skin surface. Scale bars = 50 μm.

F-J). Thus, the clinical manifestations of human DEB were reproduced in the mouse by corrective transfer of human mutated *COL7A1* gene.

Discussion

COL7 is a major component of anchoring fibril loop structures beneath the epidermal basement membrane.[12,16] Previous studies have indicated that epidermal keratinocytes are the primary source of COL7 in developing human skin.[5,6] Thus, epidermal keratinocytes have been the main focus in the development of corrective gene therapies for DEB caused by *COL7A1* mutations. However, we recently showed that gene-transferred fibroblasts can supply a larger proportion of COL7 to the new dermal-epidermal junction as efficiently as gene-transferred keratinocytes.[17] Moreover, fibroblasts are more robust and less susceptible to growth arrest and differentiation than are epidermal keratinocytes.[6] Our study is are the first *in vivo* study to show that keratinocytes and fibroblasts, through direct comparative studies, are both feasible targets for DEB gene therapy. In addition, this study can be extended to other basement membrane proteins, and fibroblasts may provide those proteins from the dermis toward the epidermis.

We first generated several transgenic mice with COL7 expression under the control of each of the following promoters: K14, col1a2, and CMV. We have shown that COL7 expression from either keratinocytes or dermal fibroblasts can be fully integrated into the epidermal BMZ *in vivo*. We have also shown that expression of COL7 by either keratinocytes or fibroblasts can successfully rescue $COL7^{m-/-}$ mice.[3] Consequently, the rescued mice ($COL7^{m-/-,\ K14\text{-}h+}$, $COL7^{m-/-,\ col1\text{-}h+}$, and $COL7^{m-/-,\ CMV\text{-}h+}$) show expression of human COL7 under the control of the different promoters. These three different rescued mouse lines show no evidence of the DEB phenotype, and their reproductive ability was restored. Ultrastructurally, newly formed anchoring fibrils were present, and the NC-1 domain of COL7 localized precisely in the lamina densa of the BMZ in the rescued mice. Collectively, these results provide future prospects for corrective gene therapy for DEB.

Generally speaking, the nature of promoters used in transgenes does not always define the amount of transgene expression in transgenic mice. In the present study, immunofluorescence and immunoblot analysis suggested that fibroblast-targeted rescued $COL7^{m-/-,\ col1\text{-}h+}$ mice expressed more human COL7 than that expressed in ubiquitous CMV promoter-driven rescued $COL7^{m-/-,\ CMV\text{-}h+}$ mice and keratinocyte-targeted rescued $COL7^{m-/-,\ K14\text{-}h+}$ mice. Interestingly, in contrast, semiquantitative morphometric analysis of anchoring fibril density revealed that anchoring fibril density was highest in the ubiquitous CMV promoter-driven rescued $COL7^{m-/-,\ CMV\text{-}h+}$ mice, among the three lines of rescued mice, although no statistically significant difference was confirmed. We cannot explain the exact mechanism behind this discrepancy. In ubiquitous CMV promoter-driven rescued $COL7^{m-/-,\ CMV\text{-}h+}$ skin, COL7 is produced by both fibroblasts and keratinocytes, similar to the physiological manner of COL7 expression. Thus, we speculate that, in $COL7^{m-/-,\ CMV\text{-}h+}$ skin, COL7 peptides might be more efficiently assembled to form anchoring fibrils, even if less protein is expressed than in the $COL7^{m-/-,\ col1\text{-}h+}$ or $COL7^{m-/-,\ K14\text{-}h+}$ skin in which COL7 is expressed only by fibroblasts or keratinocytes, respectively.

The mice developed in this study can also provide a useful model for immunobullous diseases involving COL7. Recently, we succeeded in generating a bullous pemphigoid model.[18] Passive transfer of bullous pemphigoid autoantibodies into wild-type mice has failed to induce skin lesions, because of differences between humans and mice in the amino acid sequence of the pathogenic epitope of the autoantigen, COL7.[19] We injected the patients' autoantibody into murine COL7 knockout mice that had been rescued by the expression of the human autoantigen. This resulted in successful reactions by autoantigens and autoantibodies, thereby producing the bullous pemphigoid phenotype. Epidermolysis bullosa acquisita is an autoimmune blistering disorder, and the patients' autoantibodies react to COL7. Therefore, the rescued mice with humanized COL7 that we produced should be useful in future research on epidermolysis bullosa acquisita as well.

Another interesting aspect of the present study is that we were able to develop $COL7^{K14\text{-}\Delta h+}$ transgenic mice with human *COL7A1* cDNA containing the mutation c.7528delG. The $COL7^{K14\text{-}\Delta h+}$ transgenic mice and the $COL7^{m-/-,\ K14\text{-}\Delta h+}$ rescued mice showed positive human COL7 staining at the BMZ, indicating that COL7 without the NC-2 domain can still form a triple helix and be secreted by keratinocytes. The characteristic component of all collagens is the triple helix formed by three subunits, and its assembly is based on the repetition of the Gly-X-Y repeats. It has been suggested that a zipper-like mechanism of triple helix formation starts from the C

terminus toward the N terminus in collagens I and IV[20–22] and from the N-terminal to the C-terminal direction in epidermal type XVII collagen.[23] Our experiments using the genetically engineered mouse model suggest that the N- to C-terminal mechanism of triple helix formation is also possible for COL7. However, lack of the NC-2 domain, which is critical for antiparallel-dimer formation, might cause partial and weak immunoreactivity of human COL7 in the BMZ of COL7$^{m-/-, K14\text{-}\Delta h+/+}$ mice. This study demonstrates the importance of the NC-2 domain in COL7 formation and assembly *in vivo*.

Of importance, we have generated a mouse model of DEB that allows for long-term studies that were not possible with the previously generated neonatal lethal COL7$^{m-/-}$ *col7a1* knockout mice. A surviving DEB mouse model (the mouse COL7 hypomorphic mouse) that was recently reported expresses mouse COL7 at approximately 10% of normal levels.[4] These mice could survive longer than *Col7a1* knockout mouse (COL7$^{m-/-}$) and present clinical phenotypes (mitten hands and feet) similar to those of human DEB. The phenotypes of these model mice were produced from the gene-engineered mouse COL7 gene using a hypomorphic technique. These mice had a high mortality rate (67%) within 28 days without a change to a liquid diet consisting of infant milk. On the contrary, our novel mouse models of RDEB were generated by completely different methodology using a mutated human *COL7A1* gene, and the mouse could survive longer without use of a liquid diet. Surprisingly, our original DEB model mouse is very similar to humans not only in terms of clinical manifestations but also in terms of the genetic background. In fact, the COL7$^{m-/-, K14\text{-}\Delta h+}$ mice demonstrated nail dystrophy, scarring on the paws, fusion of the digits, yellowish dental caries, and mild alopecia, even in the absence of overt blistering. The previous *col7a1* knockout COL7$^{m-/-}$ mice developed spontaneous blistering soon after birth and died within several days.[3] Thus, COL7$^{m-/-}$ mice have not been available for long-term experiments. In this study, the production of rescued mice with mutated *COL7A1* (COL7$^{m-/-, K14\text{-}\Delta h+}$) has given us a surviving model of DEB. This model has great potential for future research into the pathomechanisms of DEB, wound healing, the development of squamous cell carcinomas, and the development of molecular therapies for patients with DEB.

Although we used cDNA with the mutation c.7528delG, which causes a premature stop termination codon (PTC), the consequences of the PTC mutation in the *COL7A1* cDNA are different from those in the *COL7A1* gene. Genomic PTC mutations are subject to nonsense-mediated mRNA decay, resulting in mRNA degradation in some instances. In the literature, genomic PTC mutations in *COL7A1* were previously reported to result in nonsense-mediated mRNA decay and absence of COL7 protein synthesis in severe generalized cases of RDEB.[24,25] Whether a genomic PTC mutation leads to nonsense-mediated mRNA decay depends on the mutation site.[26] In contrast, the PTC mutation in cDNA does not lead to mRNA decay and is thought to generate a truncated protein. In fact, we confirmed the expression of human COL7 derived from human mutant *COL7A1* in the COL7$^{m-/-, K14\text{-}\Delta h+}$ mice by immunoblot analysis (data not shown) and immunofluorescence staining (Figure 6D) in the present study. Approximately 300 distinct *COL7A1* mutations have been identified in patients with DEB around the world, and the clinical features, severity, prognosis, and response to treatment vary depending on the specific mutation.[15,24,27–31] Our understanding of how specific mutations produce differing clinical presentations and prognoses is limited. We believe that our systems have the advantage of being able to use human genes. Because the COL7 gene is almost 30 kb in size, introduction of the gene with PTC mutation might be impractical. However, if we generate the same mouse models with the patient-specific missense mutations in the cDNA or with the patient-specific PTC mutation in partial genomic DNA, which was inserted in the cDNA, then they might be useful for evaluating the prognosis of each patient with a certain mutation and for developing a mutation-specific treatment. This strategy could be extended to the development of therapies tailored to other, currently intractable inherited diseases.

Acknowledgments

We thank Ms. Akari Nagasaki and Ms. Shizuka Miyakoshi for their technical assistance.

References

1. Fine JD, Eady RA, Bauer EA, Bauer JW, Bruckner-Tuderman L, Heagerty A, Hintner H, Hovnanian A, Jonkman MF, Leigh I, McGrath JA, Mellerio JE, Murrell DF, Shimizu H, Uitto J, Vahlquist A, Woodley D, Zambruno G: The classification of inherited epidermolysis bullosa (EB): Report of the Third International Consensus Meeting on Diagnosis and Classification of EB. J Am Acad Dermatol 2008, 58:931–950
2. Uitto J, Pulkkinen L: Molecular genetics of heritable blistering disorders. Arch Dermatol 2001, 137:1458–1461
3. Heinonen S, Männikkö M, Klement JF, Whitaker-Menezes D, Murphy GF, Uitto J: Targeted inactivation of the type VII collagen gene (Col7a1) in mice results in severe blistering phenotype: a model for recessive dystrophic epidermolysis bullosa. J Cell Sci 1999, 112:3641–3648
4. Fritsch A, Loeckermann S, Kern JS, Braun A, Bösl MR, Bley TA, Schumann H, von Elverfeldt D, Paul D, Erlacher M, von Rautenfeld DB, Hausser I, Fässler R, Bruckner-Tuderman L: A hypomorphic mouse model of dystrophic epidermolysis bullosa reveals mechanisms of disease and response to fibroblast therapy. J Clin Invest 2008, 118:1669–1679
5. Ryynänen J, Sollberg S, Parente MG, Chung LC, Christiano AM, Uitto J: Type VII collagen gene expression by cultured human cells and in fetal skin: abundant mRNA and protein levels in epidermal keratinocytes. J Clin Invest 1992, 89:163–168
6. Goto M, Sawamura D, Ito K, Abe M, Nishie W, Sakai K, Shibaki A, Akiyama M, Shimizu H: Fibroblasts show more potential as target cells than keratinocytes in COL7A1 gene therapy of dystrophic epidermolysis bullosa. J Invest Dermatol 2006, 126:766–772
7. Ortiz-Urda S, Lin Q, Green CL, Keene DR, Marinkovich MP, Khavari PA: Injection of genetically engineered fibroblasts corrects regenerated human epidermolysis bullosa skin tissue. J Clin Invest 2003, 111:251–255
8. Woodley DT, Krueger GG, Jorgensen CM, Fairley JA, Atha T, Huang Y, Chan L, Keene DR, Chen M: Normal and gene-corrected dystrophic epidermolysis bullosa fibroblasts alone can produce type VII collagen at the basement membrane zone. J Invest Dermatol 2003, 121:1021–1028
9. Wong T, Gammon L, Liu L, Mellerio JE, Dopping-Hepenstal PJ, Pacy J, Elia G, Jeffery R, Leigh IM, Navsaria H, McGrath JA: Potential of

fibroblast cell therapy for recessive dystrophic epidermolysis bullosa. J Invest Dermatol 2008, 128:2179–2189
10. Shibaki A, Sato A, Vogel JC, Miyagawa F, Katz SI: Induction of GVHD-like skin disease by passively transferred $CD8^+$ T-cell receptor transgenic T cells into keratin 14-ovalbumin transgenic mice. J Invest Dermatol 2004, 123:109–115
11. Denton CP, Zheng B, Shiwen X, Zhang Z, Bou-Gharios G, Eberspaecher H, Black CM, de Crombrugghe B: Activation of a fibroblast-specific enhancer of the proalpha2(I) collagen gene in tight-skin mice. Arthritis Rheum 2001, 44:712–722
12. Shimizu H, Ishiko A, Masunaga T, Kurihara Y, Sato M, Bruckner-Tuderman L, Nishikawa T: Most anchoring fibrils in human skin originate and terminate in the lamina densa. Lab Invest 1997, 76:753–763
13. Sawamura D, Mochitomi Y, Kanzaki T, Nakamura H, Shimizu H: Glycine substitution mutations by different amino acids at the same codon in *COL7A1* cause different modes of dystrophic epidermolysis bullosa inheritance. Br J Dermatol 2006, 155:834–837
14. Shimizu H, McGrath JA, Christiano AM, Nishikawa T, Uitto J: Molecular basis of recessive dystrophic epidermolysis bullosa: genotype/phenotype correlation in a case of moderate clinical severity. J Invest Dermatol 1996, 106:119–124
15. Sawamura D, Goto M, Yasukawa K, Sato-Matsumura K, Nakamura H, Ito K, Nakamura H, Tomita Y, Shimizu H: Genetic studies of 20 Japanese families of dystrophic epidermolysis bullosa. J Hum Genet 2005, 50:543–546; erratum in J Hum Genet 2006, 51:839)
16. Uitto J, Chung-Honet LC, Christiano AM: Molecular biology and pathology of type VII collagen. Exp Dermatol 1992, 1:2–11
17. Woodley DT, Keene DR, Atha T, Huang Y, Ram R, Kasahara N, Chen M: Intradermal injection of lentiviral vectors corrects regenerated human dystrophic epidermolysis bullosa skin tissue in vivo. Mol Ther 2004, 10:318–326
18. Nishie W, Sawamura D, Goto M, Ito K, Shibaki A, McMillan JR, Sakai K, Nakamura H, Olasz E, Yancey KB, Akiyama M, Shimizu H: Humanization of autoantigen. Nat Med 2007, 13:378–383
19. Liu Z, Diaz LA, Troy JL, Taylor AF, Emery DJ, Fairley JA, Giudice GJ: A passive transfer model of the organ-specific autoimmune disease, bullous pemphigoid, using antibodies generated against the hemidesmosomal antigen. BP180 J Clin Invest 1993, 92:2480–2488
20. Engel J, Prockop DJ: The zipper-like folding of collagen triple helices and the effects of mutations that disrupt the zipper. Annu Rev Biophys Biophys Chem 1991, 20:137–152
21. Beck K, Boswell BA, Ridgway CC, Bächinger HP: Triple helix formation of procollagen type I can occur at the rough endoplasmic reticulum membrane. J Biol Chem 1996, 271:21566–21573
22. Söder S, Pöschl E: The NC1 domain of human collagen IV is necessary to initiate triple helix formation. Biochem Biophys Res Commun 2004, 325:276–280
23. Areida SK, Reinhardt DP, Muller PK, Fietzek PP, Kowitz J, Marinkovich MP, Notbohm H: Properties of the collagen type XVII ectodomain: evidence for N- to C-terminal triple helix folding. J Biol Chem 2001, 276:1594–1601
24. Hilal L, Rochat A, Duquesnoy P, Blanchet-Bardon C, Wechsler J, Martin N, Christiano AM, Barrandon Y, Uitto J, Goossens M, Hovnanian A: A homozygous insertion-deletion in the type VII collagen gene (COL7A1) in Hallopeau-Siemens dystrophic epidermolysis bullosa. Nat Genet 1993, 5:287–293
25. Hovnanian A, Rochat A, Bodemer C, Petit E, Rivers CA, Prost C, Fraitag S, Christiano AM, Uitto J, Lathrop M, Barrandon Y, de Prost Y: Characterization of 18 new mutations in COL7A1 in recessive dystrophic epidermolysis bullosa provides evidence for distinct molecular mechanisms underlying defective anchoring fibril formation. Am J Hum Genet 1997, 61:599–610
26. Lejeune F, Maquat LE: Mechanistic links between nonsense-mediated mRNA decay and pre-mRNA splicing in mammalian cells. Curr Opin Cell Biol 2005, 17:309–315
27. Mellerio JE, Dunnill MG, Allison W, Ashton GH, Christiano AM, Uitto J, Eady RA, McGrath JA: Recurrent mutations in the type VII collagen gene (COL7A1) in patients with recessive dystrophic epidermolysis bullosa. J Invest Dermatol 1997, 109:246–249
28. Pulkkinen L, Uitto J: Mutation analysis and molecular genetics of epidermolysis bullosa. Matrix Biol 1999, 18:29–42
29. Gardella R, Castiglia D, Posteraro P, Bernardini S, Zoppi N, Paradisi M, Tadini G, Barlati S, McGrath JA, Zambruno G, Colombi M: Genotype-phenotype correlation in Italian patients with dystrophic epidermolysis bullosa. J Invest Dermatol 2002, 119:1456–1462
30. Kern JS, Kohlhase J, Bruckner-Tuderman L, Has C: Expanding the COL7A1 mutation database: novel and recurrent mutations and unusual genotype-phenotype constellations in 41 patients with dystrophic epidermolysis bullosa. J Invest Dermatol 2006, 126:1006–1012
31. Varki R, Sadowski S, Uitto J, Pfendner E: Epidermolysis bullosa. II. Type VII collagen mutations and phenotype-genotype correlations in the dystrophic subtypes. J Med Genet 2007, 44:181–192

Cell

Genotoxic Stress Abrogates Renewal of Melanocyte Stem Cells by Triggering Their Differentiation

Ken Inomata,[1,2,3] Takahiro Aoto,[1,4] Nguyen Thanh Binh,[1] Natsuko Okamoto,[1,5] Shintaro Tanimura,[1,3] Tomohiko Wakayama,[6] Shoichi Iseki,[6] Eiji Hara,[7] Takuji Masunaga,[2] Hiroshi Shimizu,[3] and Emi K. Nishimura[1,4,*]

[1]Division of Stem Cell Medicine, Center for Cancer and Stem Cell Research, Cancer Research Institute, Kanazawa University, 13-1 Takaramachi, Kanazawa, Ishikawa 920-0934, Japan

[2]Fundamental Research Laboratories, KOSÉ Corporation, 1-18-4 Azusawa, Itabashi-ku, Tokyo 174-0051, Japan

[3]Department of Dermatology, Hokkaido University Graduate School of Medicine, North 15 West 7, Kita-ku, Sapporo 060-8638, Japan

[4]Department of Stem Cell Biology, Medical Research Institute, Tokyo Medical and Dental University, 2-3-10 Kandasurugadai, Chiyoda-ku, Tokyo 101-0062, Japan

[5]Department of Dermatology, Kyoto University Graduate School of Medicine, 54 Shogoin-Kawaharacho, Sakyo-Ku, Kyoto, 606-8507, Japan

[6]Department of Histology and Embryology, Graduate School of Medical Science, Kanazawa University, 13-1 Takara-machi, Kanazawa, Ishikawa 920-0934, Japan

[7]Division of Cancer Biology, The Cancer Institute, Japanese Foundation for Cancer Research, 3-10-6, Ariake, Koto-ku, Tokyo 135-8550, Japan

*Correspondence: nishscm@tmd.ac.jp

DOI 10.1016/j.cell.2009.03.037

SUMMARY

Somatic stem cell depletion due to the accumulation of DNA damage has been implicated in the appearance of aging-related phenotypes. Hair graying, a typical sign of aging in mammals, is caused by the incomplete maintenance of melanocyte stem cells (MSCs) with age. Here, we report that irreparable DNA damage, as caused by ionizing radiation, abrogates renewal of MSCs in mice. Surprisingly, the DNA-damage response triggers MSC differentiation into mature melanocytes in the niche, rather than inducing their apoptosis or senescence. The resulting MSC depletion leads to irreversible hair graying. Furthermore, deficiency of Ataxia-telangiectasia mutated (ATM), a central transducer kinase of the DNA-damage response, sensitizes MSCs to ectopic differentiation, demonstrating that the kinase protects MSCs from their premature differentiation by functioning as a "stemness checkpoint" to maintain the stem cell quality and quantity.

INTRODUCTION

Stem cell systems maintain the homeostasis of tissues, which are constantly subjected to genotoxic stress such as that caused by reactive metabolic byproducts and environmental mutagens. The accumulation of somatic DNA damage is now considered a main cause of the aging process in multicellular organisms (Hasty et al., 2003; Schumacher et al., 2008). Stem cell depletion due to the accumulation of DNA damage has been reported in animals with genomic instability and has been implicated in the decline of tissue renewal capacity and the appearance of aging-related phenotypes (Nijnik et al., 2007; Rossi et al., 2007a; Ruzankina et al., 2007). Stem cell senescence and/or apoptosis are thought to be two major cellular mechanisms for stem cell depletion following DNA damage (Ruzankina et al., 2008; Sharpless and DePinho, 2007). p53 and $p16^{Ink4a}$ are the best characterized regulators of senescence and apoptosis in response to DNA damage, including oncogenic mutations, and have been implicated as "gatekeepers" for tumor suppression as well as in tissue aging (Campisi, 2003a; Lowe et al., 2004; Maier et al., 2004; Sharpless and DePinho, 2007).

Hair graying is one of the most obvious sign of aging. Melanogenesis resulting in hair pigmentation is tightly coupled with the hair regeneration cycle. Hair follicles are constantly renewed by altering phases of growth (anagen), regression (catagen), and rest (telogen) (Figure S1 available online). Hair pigments are produced by differentiated melanocytes in the hair matrix during anagen. Melanocyte maturation is mediated by a lineage differentiation program involving MITF, the master transcriptional regulator for melanocyte development, and its target genes responsible for melanin pigment synthesis (Levy et al., 2006; Vance and Goding, 2004). α-melanocyte-stimulating hormone (MSH) signaling through its receptor melanocortin 1 receptor (MC1R) upregulates MITF to stimulate melanogenesis and eumelanin (black/brown) pigment synthesis (Hearing, 2005; Levy et al., 2006; Yamaguchi et al., 2007). Mature melanocytes required for hair pigmentation are supplied from the melanocyte stem cell (MSC) population. We previously identified immature Dct-lacZ^{+}/KIT^{low} melanoblasts located in the bulge area of hair follicles as MSCs (Nishimura et al., 2002, 2005). The MSC population is maintained in that niche environment throughout the hair cycle and self-renews only at early anagen to provide amplifying and differentiating progenies to the hair matrix for hair pigmentation (Figures 2U and S1) (Nishimura et al., 2002). Furthermore, maintenance of this MSC population becomes incomplete with aging, causing physiological hair graying (Nishimura et al., 2005).

Interestingly, the onset of hair graying is preceded by the appearance of ectopically pigmented melanocytes (EPMs), which have a dendritic morphology, in the niche, suggesting that MSCs are differentiated in the niche (Nishimura et al., 2005). As the stem cell niche is occupied by immature MSCs in non-aged physiological conditions, the appearance of EPMs in the stem cell niche is a distinctive event. However, the cause(s) underlying the aging phenomenon and the possible involvement of the DNA-damage response in the appearance of EPMs have not been studied.

Premature hair graying is seen in progeroid syndromes such as Werner's syndrome and Ataxia-telangiectasia (AT) (Hasty et al., 2003; Martin, 2005) as well as after ionizing radiation (IR) (Cooldige, 1925), which damages DNA and causes DNA double-strand breaks (Ward, 1988). Inactivation of "caretaker genes," including *ATM* (ataxia telangiectasia mutated), a kinase which is a key DNA-damage sensor/transducer, causes genomic instability due to an inefficient DNA-damage response (DDR) and results in progeria that segmentally mimics physiological aging (Kinzler and Vogelstein, 1998; McKinnon, 2004; van Heemst et al., 2007). Indeed, AT patients exhibit premature hair graying (Boder and Sedgwick, 1970; Martin, 2005; Taylor et al., 1975), and ATM deficiency in mice also accelerates IR-induced hair graying (Barlow et al., 1999).

In this study, we examined the impact of DNA damage in quiescent MSCs in vivo and the role of caretaker and gatekeeper genes in the determination of the fate of damaged stem cells as well as the involvement of DNA damage in the hair graying phenotype. Our chronological fate analysis of MSCs revealed that they lose their stem cell immaturity and commit to differentiation in the niche after exposure to excessive genotoxic stress, which results in stem cell depletion and subsequent hair graying. Our results indicate that the MSC system maintains the quality of the stem cell pool by eliminating damaged stem cells via the induction of stem cell differentiation in the niche.

RESULTS

Genotoxic Stress Induces the Ectopic Differentiation of MSCs in the Niche

We explored the effects of IR on the coat color of adult mice. At least 5 Gy of IR on the skin was necessary and sufficient for the stable induction of hair graying (Figures 1A and 1B). Next, to determine whether 5 Gy of IR induces any changes in MSCs preceding the onset of hair graying, we examined the morphological changes of the MSC population using expression of the *Dct-lacZ* transgene that tags the melanocyte lineage or another melanocyte lineage marker, KIT. In control nonirradiated mice, Dct-lacZ$^+$ melanoblasts in the hair follicle bulge, which we previously identified as MSCs (Nishimura et al., 2002), were unpigmented with oval and small cell bodies and coexpressed Kit during anagen (Figures 1C, 1D, and 1F) (Nishimura et al., 2005). In sharp contrast, EPMs with dendritic morphologies, instead of immature melanoblasts, appeared in the bulge area of mid-anagen hair follicles after IR (Figures 1G–1J). Most of the EPMs also expressed Dct-lacZ and KIT (Figures 1H–1J). These changes were followed by the significant loss of differentiated melanocytes in the hair matrix in the following hair cycles and resultant depigmentation of newly grown hair (Figures 1B and 1L).

The appearance of EPMs in the niche and the subsequent hair graying were reproducibly induced by 5 Gy IR and most efficiently when the mice were irradiated at around 7–8 weeks after birth, when most hair follicles on the trunk are well synchronized at the resting stage (telogen). The fact that quiescent MSCs but not their amplifying or differentiated progeny reside in these telogen hair follicles enabled us to selectively chase the fate of MSCs in the niche by irradiating at telogen phase. Synchronous stimulation of hair-cycle progression by the telogen-hair plucking method (Potten, 1970) allowed us to further analyze the chronological changes of MSCs after their synchronized activation at the beginning of the hair growth stage (at 2 days after hair plucking) (Figures 2A–2U and S2C). The activated MSCs self-renew transiently only at anagen II and are maintained in a quiescent (noncycling) state throughout the rest of hair follicle cycle both with or without hair plucking (Nishimura et al., 2002) (Figure S1 and data not shown). IR with hair plucking did not result in any detectable differences from IR without hair plucking regarding the fate of MSCs and the resulting coat color of newly regenerated hair (Figures S3, 1B, and 1G–1J). Furthermore, telogen-hair plucking made it efficient to assess the color of newly grown hair without waiting for the previous hair to fall off. Thus, we took advantage of this chronological analysis method in subsequent experiments to examine the effects of IR on quiescent MSCs and to efficiently trace their fate throughout the hair-cycle progression. As shown in Figure 2, Dct-lacZ$^+$ cells in the bulge (MSCs) of irradiated mice keep their dendritic morphology after their division at anagen II and begin to produce abundant pigments in the cytoplasm along with the hair-cycle progression (Figures 2M, 2N, 2R, and 2S). Those dendritic EPMs in the bulge area of follicles at anagen IV and V mimic exactly the EPMs that we previously found in the MSC niche in aging whisker hair follicles (Nishimura et al., 2005) (Figure 1X). EPMs were induced within the bulge area only after stem cell division but MSCs were kept unpigmented while the follicles remained in telogen even after IR (Figures S3G–S3J and data not shown), suggesting that the preceding stem cell activation at early anagen or stem cell division is necessary for the ectopic pigmentation of MSCs in the niche. Furthermore, all these EPM populations in the niche were negative for CD11b/MAC1, a marker for mature myelomonocytic cells, thus being distinguished from macrophages, and eventually disappeared specifically at anagen VI due to their phagocytosis by surrounding keratinocytes (Figures 2O, 2T, S4, and S5).

To examine the relationship between these changes in MSCs and the color of regenerated hair in subsequent hair cycles, we looked at MSCs in the next hair cycle histologically and the consequent hair pigmentation. MSCs were undetectable in the hair follicle bulge in the following cycle and the hair was unpigmented (Figures 1K–1N). The appearance of EPMs in mid-anagen and the consequent depletion of MSCs in the niche at late anagen led to the depigmentation of newly grown hair (Figures 1K–1O and 1B). Therefore, we conclude that IR abrogates renewal of MSCs by inducing their differentiation in the niche, which causes their depletion and leads to hair depigmentation in subsequent hair cycles.

To test whether pigmentation of MSCs can be commonly induced by other DNA-damage inducers, we treated mice with different genotoxic reagents, including busulfan, mitomycin C,

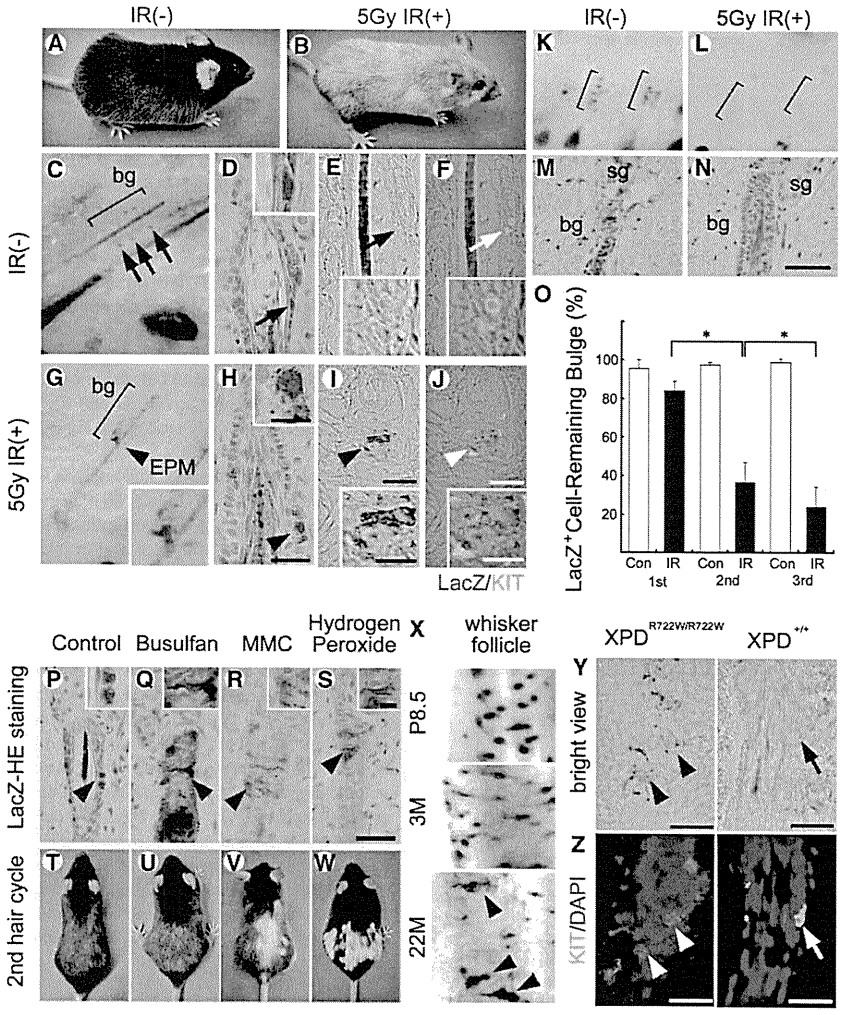

Figure 1. Genotoxic Stress Induces Ectopic Pigmentation of MSCs in the Niche

(A and B) The coat color of control (IR(−)) and X-ray irradiated (5Gy IR(+)) C57BL/6J mice. Hair graying is induced after IR.

(C–J) Histological changes in irradiated hair follicles at anagen V. The bulge areas (bg) of hair follicles on the trunk skin are shown. Whole-mount (C and G) and sectioned lacZ-stained skin from *Dct-lacZ* transgenic mice (D and H). lacZ$^+$ unpigmented melanoblasts (MSCs) were found in the bulge areas of control hair follicles (blue cells with arrows in C and D). (E, F, I, and J) lacZ$^+$ cells (red) in the hair follicle bulge, which coexpress KIT (green), contain no pigment without IR (arrows in E and F) while containing brown-black pigment after IR (arrowheads in I and J) in the bright field view. EPMs with dendritic morphology instead of unpigmented melanoblasts with small and round cell bodies were found in the bulge at 7 days after 5 Gy IR (arrowheads, EPM) (I and J).

(K–N) Disappearance of lacZ$^+$ cells in the hair follicle bulge in the 2nd hair cycle after IR. Whole-mount (K and L) and sectioned lacZ-stained (M and N) skins from control (K and M) and irradiated mice (L and N). Brackets indicate the bulge (bg) areas (K and L).

(O) The frequency of hair follicles that still contain any lacZ$^+$ cells including EPMs in the bulge per total hair follicles in the 1st, 2nd, and 3rd hair cycles after IR.

(P–S) Histological changes in hair follicle bulge areas after treatment with genotoxic reagents. Induction of EPM at 6 days after treatment with busulfan (40 mg/kg body weight) (Q), MMC (Mitomycin C: 4 mg/kg body weight) (R), or hydrogen peroxide (1% in PBS) (S), but not with control vehicle (P). The insets show magnified views of lacZ$^+$ cells indicated by the arrowheads.

(T–W) White hair growth in the 2nd hair cycle after treatment with different genotoxic reagents (U, V, and W) but not with control (T).

(X) Whole-mount lacZ staining of lower permanent portion of whisker hair follicles (stem cell niche) of *Dct-lacZ* transgenic mice at different ages. EPMs with dendritic morphology are found in the niche of aged follicles (22 M, arrowhead).

(Y and Z) The bulge areas of XPD$^{R722W/R722W}$ and XPD$^{+/+}$ 42-week-old mice. KIT$^+$ cells (Z, green) in the hair follicle bulge contain pigment in XPD$^{R722W/R722W}$ mice (arrowheads) but not in control mice (arrows in XPD$^{+/+}$) (Y).

Error bars represent standard error of the mean (SEM); *$p < 0.001$ as calculated by Student's t test. Scale bars represent 25 μm in (H), (I), and (J), 50 μm in (N) and (S), and 10 μm in the insets of (H), (I), (J), and (S). Abbreviations: bg, bulge; sg, sebaceous gland; P, postnatal day; M, month.

and hydrogen peroxide. Local administration of those genotoxic reagents similarly induced EPMs in the bulge and resulted in hair graying in the subsequent hair cycles (Figures 1P–1W). The amount of EPMs in the bulge and the resulting hair depigmentation in subsequent hair cycles varied depending on the chemicals, doses, and skin areas tested (Figures 1U–1W) compared to IR, which induces hair graying and EPMs much more evenly over the entire skin. To further test whether EPMs can be triggered by endogenous DNA damage, we analyzed the hair follicle bulge in XPD$^{R722W/R722W}$ trichothiodystrophy (TTD) mice, which show premature aging phenotypes, such as hair graying (de Boer et al., 2002), that are associated with genetically impaired DNA repair.

EPMs were sporadically found in the bulge area of mid-anagen follicles in XPD$^{R722W/R722W}$ but not in control XPD$^{+/+}$ mice (Figures 1Y and 1Z), suggesting that endogenous DNA damage also triggers the phenomenon. Collectively, these data show that the renewal of MSCs becomes defective with different kinds of genotoxic stress and that the consequent depletion of MSCs causes subsequent hair graying. As the MSC changes and the processes were not distinguishable from the IR-induced EPMs, we further analyzed this phenomenon in *Dct-lacZ* transgenic mice using IR, which induces EPMs and hair graying most efficiently.

DNA-Damage Response in MSCs

To determine whether the DDR is activated in MSCs after IR, we used fluorescent immunohistochemistry to examine foci formation of phosphorylated H2AX (γH2AX), 53BP1, and phosphorylated ATM in hair follicles. We find that DNA-damage foci

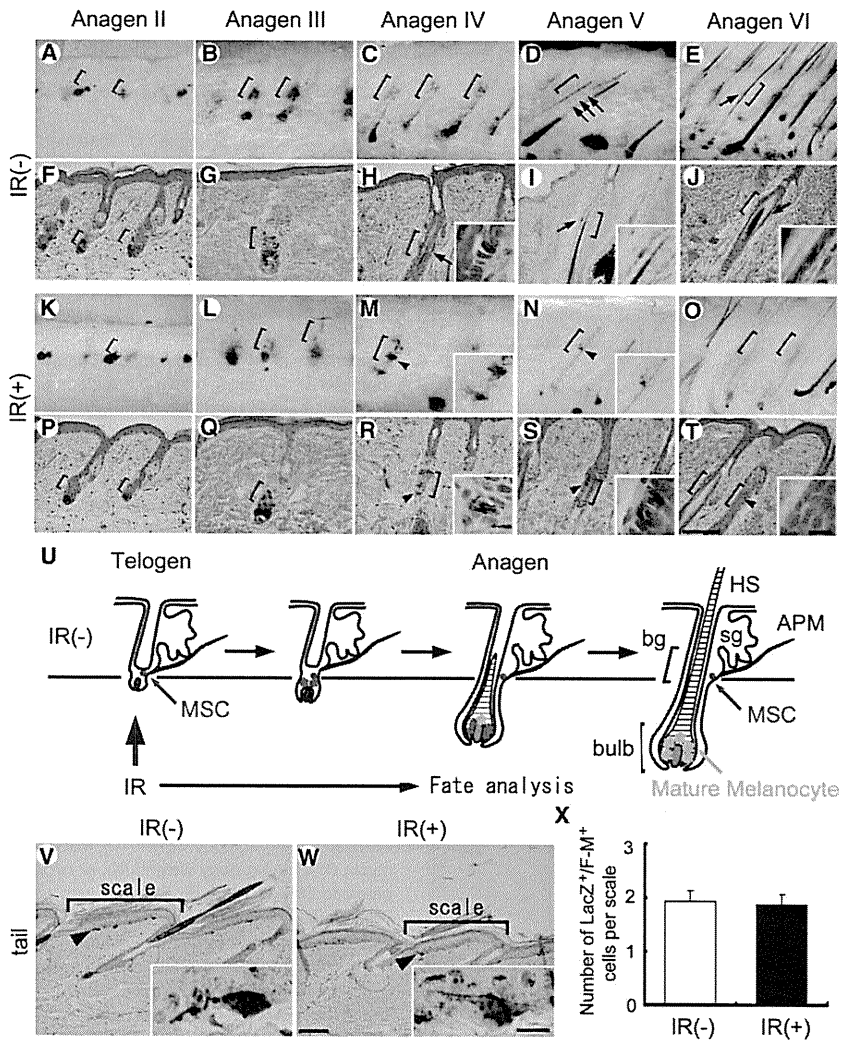

Figure 2. IR Induction of Ectopic Pigmentation and Subsequent Depletion of MSCs in the Niche in Synchronization with Hair-Cycle Progression

Distribution and morphological changes of Dct-lacZ$^+$ cells in irradiated (IR (+)) and control (IR (–)) hair follicles during hair-cycle progression in *Dct-lacZ* transgenic mice. Hair-cycle synchronization was induced by telogen-hair plucking at 7 weeks after birth.

(A–T) Whole-mount (A–E, K–O) and sectioned lacZ-stained skin (F–J, P–T) of *Dct-lacZ* transgenic mice with or without IR. Arrows show lacZ$^+$ cells in bulge area (brackets). EPMs (arrowheads) were observed in the bulge area at anagen IV (M and R) and anagen V (N and S) but disappeared from the bulge area by anagen VI (O and T). Insets show magnified views of lacZ$^+$ cells indicated by the arrows or arrowheads.

(U) A schematic for the MSC fate analysis (shown in A–T) with or without IR at telogen phase.

(V, W, and X) Effects of 5 Gy IR on epidermal melanocytes (lacZ$^+$, blue) in the tail skin of mice that were processed for the above experiments for anagen IV and V follicles. Epidermal melanocytes (lacZ$^+$, blue) in the tail skin are moderately pigmented and did not show any significant changes either in cellular morphology or in pigmentation level with or without IR. The number of lacZ$^+$ Fontana-Masson$^+$ (F-M$^+$) cells per scale (brackets in V and W) are shown in (X). Epidermal melanocytes (V and W) in the hairless skin were refractory to ectopic pigmentation and subsequent disappearance (X). Insets show the magnified views of lacZ$^+$ F-M$^+$ cells indicated by the arrowheads. Scale bars represent 100 μm in (T) and (W) and 10 μm in the insets of (T) and (W). Abbreviations: bg, bulge; sg, sebaceous gland; HS, hair shaft; APM, arrector pili muscle. Error bars in (X) represent SEM.

were induced in the nuclei of cells in hair follicles after IR. Those foci appeared within 3 hr after 5 Gy IR in KIT$^+$ melanoblasts as well as in KIT$^-$ keratinocytes surrounding the bulge area, demonstrating that cells in the bulge area, including MSCs, respond to IR-induced genomic damage (Figure 3). Furthermore, the DNA-damage foci were retained in the nuclei 6 hr after IR followed by a gradual reduction in their number and intensity (Figures 3F, 3H, 3K, and 3L and data not shown). It is notable that some pigmented melanocytes in the niche retain γH2AX foci even at anagen IV (Figures 3K and 3L). These findings suggest that MSCs that incur irreparable levels of IR-induced DNA damage or an excessive DDR have committed to differentiation in the niche.

MSC Commitment to Differentiation Is a Dominant Distinct Fate under Genotoxic Stress

Apoptosis or cellular senescence are two representative cell fates in response to irreparable DNA damage or stress (Campisi, 2003b; Lowe et al., 2004). Our chronological histological analysis showed that Dct-lacZ$^+$ melanocytes are maintained in the bulge area after IR, without showing any histological signs of apoptosis. Indeed, no significant increase of cleaved caspase 3 or TUNEL positivity was found in the skin, including in the bulge area of these follicles, at any time points tested after 5 Gy IR, a dose that is sufficient to induce hair graying (Figures 4A–4C and S6). These data indicate that apoptosis is not likely to be the major early fate of DNA-damaged MSCs.

A senescence-like cellular state in vivo has been demonstrated in human nevi (moles), benign tumors of melanocytes, using senescence-associated β-galactosidase (SA-β-gal) activity and p16^{INK4A} expression as markers (Gray-Schopfer et al., 2006; Michaloglou et al., 2005). We checked SA-β-gal and p16^{INK4A} expression in mouse skin treated with IR to look for signs of a senescence-like phenotype but found neither SA-β-gal nor p16^{INK4A} in the EPMs (Figures 4D–4F, S7B, and S7D). In contrast, a human melanocytic nevus showed SA-β-gal and p16^{INK4A} expression supporting its senescence-like features (Figures 4F, S7E, and S7F), as reported previously (Gray-Schopfer et al., 2006; Michaloglou et al., 2005). These data suggest that neither cellular senescence nor apoptosis is likely to be the major fate of damaged MSCs.

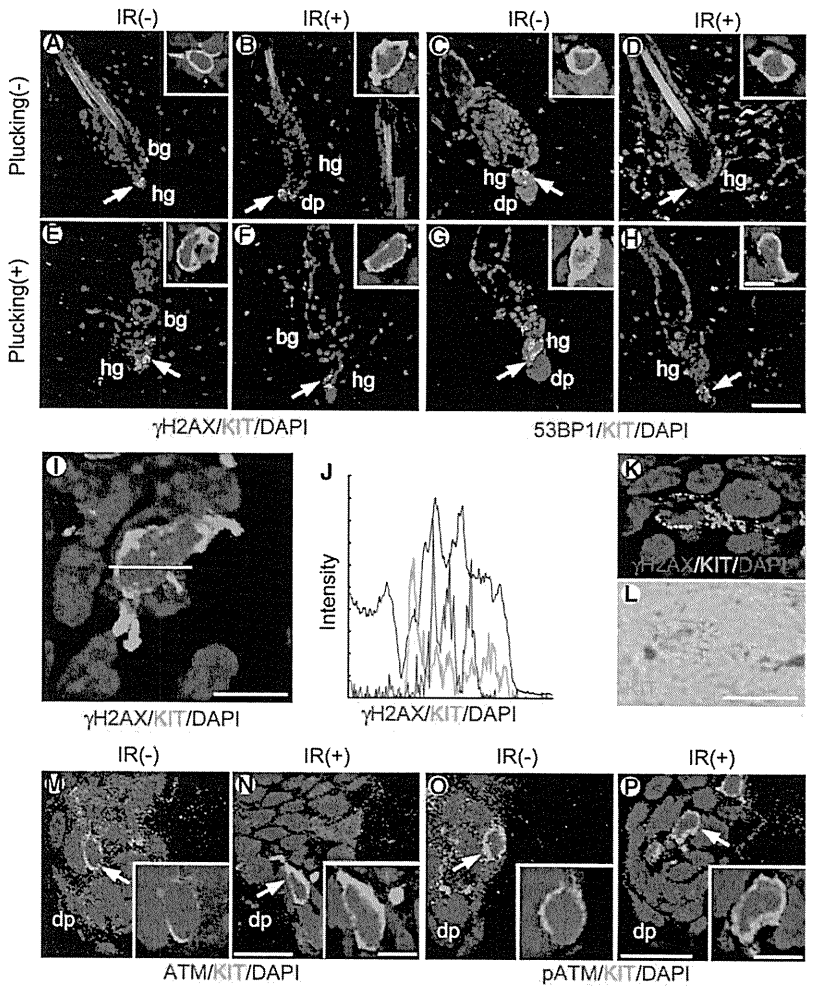

Figure 3. IR Induces DNA-Damage Foci Formation and ATM Activation in the Hair Follicle Bulge

Immunohistochemical analysis for γH2AX, 53BP1, ATM, and p-ATM expression in the hair follicle bulge. Seven-week-old mouse skin, in which almost all hair follicles are synchronized at telogen phase, was irradiated with or without hair plucking and was excised 6 hr after IR.

(A–D) Telogen follicles without IR (control) (A and C) and 6 hr after IR (B and D).

(E–H) Follicles at 1 day after plucking without IR (control) (E and G) and 6 hr after IR (F and H). The distribution of IR-induced DNA-damage foci was indistinguishable in the bulge areas including KIT^+ cells with or without plucking (B, F, D, and H, arrows).

(I) The magnified view of IR-induced γH2AX foci.

(J) Line scan showing fluorescence intensity along the white line overlying the image shown in (I). γH2AX foci (red) were found in the nuclei (blue) of KIT^+ cells (green). Lines were drawn across the nuclei through the foci of KIT^+ cells.

(K and L) IR-induced γH2AX foci remain in KIT^+ EPMs in the bulge area even in mid-anagen follicles (anagen IV). Merged image of the bright field view and KIT immunostaining is shown (L).

(M and N) Expression pattern and subcellular localization of ATM in the hair follicle bulge (arrow). ATM was broadly expressed in the bulge areas including KIT^+ MSCs (arrow) and was mainly localized to the cytoplasm without IR (M). IR induction of ATM localization in the nuclei was found in the bulge cells including KIT^+ cells (arrow) (N).

(O and P) The distribution of p-ATM foci in the bulge area. p-ATM foci were found in the nuclei of bulge cells including KIT^+ cells (arrow) only after IR.

Abbreviations: bg, bulge; dp, dermal papilla; hg, hair germ. Scale bars represent 50 μm in (H), 10 μm in the inset of (H), 10 μm in (I), 5 μm in (L), 15 μm in (N) and (P), and 5 μm in the insets of (N) and (P).

p53 or $p16^{INK4a}$-Rb pathways have been implicated in the fate determination of cells under genotoxic stress including IR (Itahana et al., 2004; Sharpless and DePinho, 2007). To assess the involvement of p53 or $p16^{INK4a}$ pathways in IR induction of EPMs in the niche, we examined expression of p53 and $p16^{INK4a}$ in the bulge after IR. IR induction of p53 expression was transiently detected in Dct-lacZ$^+$ cells in the bulge as well as in the surrounding keratinocytes during early-mid anagen but not at later stages including EPMs (Figures S7H–S7O); $p16^{INK4a}$ expression did not show significant changes with or without IR (Figures S7A–S7D).

We treated *Trp53*$^{-/-}$ and *Ink4a-Arf*$^{-/-}$ mice with IR to test whether p53, $p19^{ARF}$, or $p16^{INK4a}$ are critical for IR induction of EPMs in the niche. EPMs were found in the hair follicle bulge regions in those deficient mice, as seen in wild-type or heterozygous mice (Figures 4H–4K and 4M–4P). Furthermore, the irradiated mutant mice showed hair graying with no significant difference in appearance from their control wild-type and heterozygous mice (Figures 4G and 4L). These findings indicate that p53, $p19^{ARF}$, and $p16^{INK4a}$ are not required for ectopic differentiation of MSCs in the niche and resulting hair graying. These findings also suggest that the IR-induced fate of MSCs is distinct from cellular senescence or apoptosis and is mediated by different signaling pathways.

Genotoxic Stress Triggers the Melanocyte Differentiation Program with Prolonged Activation of Melanocyte Master Regulator MITF in MSCs

As EPMs are mostly dendritic in morphology and are well pigmented, we considered the possibility that genotoxic stress triggers MSC differentiation ectopically through the canonical differentiation program of the melanocyte lineage in the niche. We first examined the expression after IR of the master regulator of the melanocyte lineage, MITF, and downstream melanogenic enzymes, including tyrosinase (TYR) and tyrosinase-related protein 1 (TYRP1), in KIT^+ cells in the bulge area (Figures 5A–5F). In nonirradiated controls, these genes are expressed transiently by MSC progeny in the bulge area after stem cell division at early anagen (anagen II), and their expression becomes downregulated by mid-anagen (anagen IV) (Figures 5A–5C). In contrast, gene expression was prolonged in the stem cell progeny in the bulge areas of IR-radiated follicles

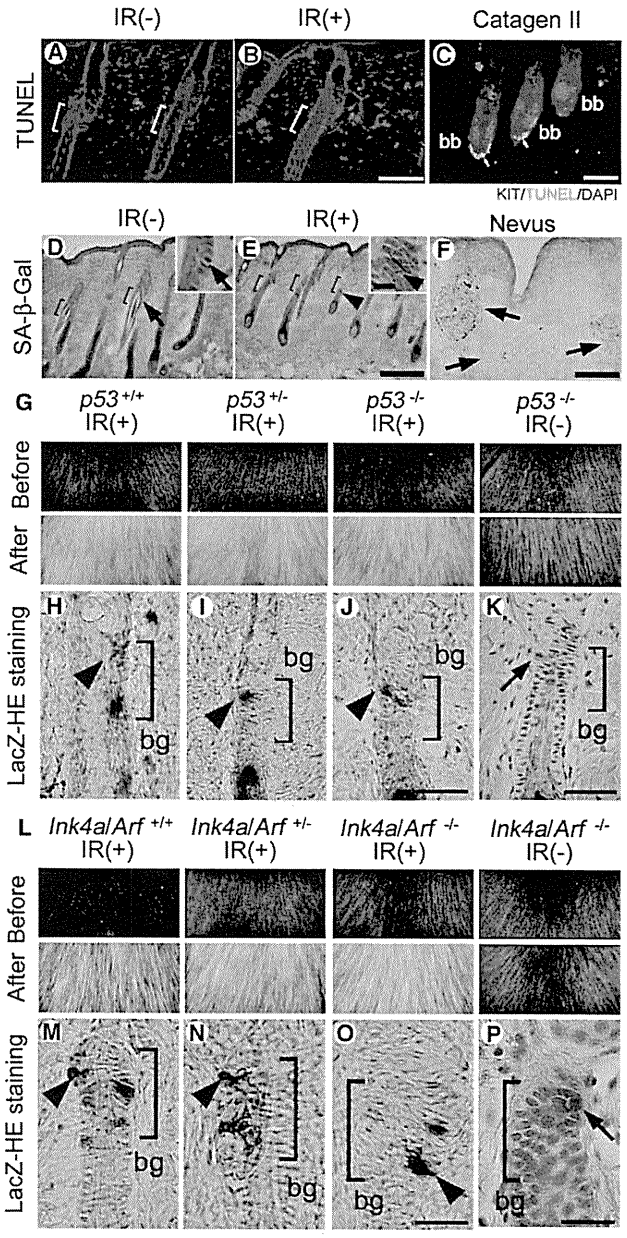

Figure 4. Appearance of EPMs Is Distinct from Apoptotic/Senescence Response and Does Not Require *p53* or *Ink4a/Arf*

(A–C) TUNEL staining of trunk skin from wild-type mice with (B) or without IR (A) and of a catagen II hair follicle as a positive control (C, arrows). TUNEL activity was not found in the hair follicle bulges (brackets) after IR (B). See Figure S6 for more details.

(D–F) Senescence-associated (SA) β-Gal staining of trunk skin from wild-type mice with (E) or without IR (D) and of a human nevus as a positive control (F, arrows). SA-β-Gal activity was not found in EPMs (arrowheads) of hair follicle bulges after IR (E).

(G–P) Effects of IR on MSCs and hair graying in *p53* (G–K) and *Ink4a-Arf*-deficient mice (L–P). (G and L) Changes of coat color before (upper) and after (lower) IR. Hair graying was similarly induced independent of the genetic background of *p53* (G) or *Ink4a/ARF* (L) status. (H–K and M–P) lacZ-stained sections of irradiated (H–J and M–O) or nonirradiated (K and P) hair follicles at anagen IV of various genotypes with *Dct-lacZ* transgene. EPMs were similarly found in the bulge areas in all genotypes (H–J and M–O, arrowheads) after IR. Coat color and MSCs (arrows) in the bulge area of *p53* (K) or *Ink4a/ARF* (P) deficient mice show no overt phenotypes without IR.

The scale bars represent 200 μm in (E) and (F), 10 μm in the inset of (E), 50 μm in (B), (C), (J), and (K), and 25 μm in (O) and (P).

(Figures 5D–5F). These results suggest that MSCs initiate differentiation in the niche via the canonical signaling pathways for melanocyte lineage differentiation.

To test whether the IR induction of melanocyte differentiation is a specific event in activated MSCs in the niche, we examined the differentiation status after IR of epidermal melanocytes located in the basal layer of the epidermis in hairless skin areas such as the tail. We found no differences in the melanin content in lacZ$^+$ epidermal melanocytes with or without 5 Gy IR (Figures 2V–2X). We thus conclude that the induction of EPM is a specific event in activated MSCs at early anagen or is due to their niche microenvironment. As IR induction of melanocyte differentiation was detectable in vitro but less frequently and at lower levels (Figure S8) than seen in activated MSCs, it is likely that the niche microenvironment of early anagen follicles, which usually supports MSC renewal, stimulates the endogenous differentiation program.

Melanosome Formation and Maturation in the Niche

The function of mature melanocytes in the skin is to produce melanin pigments, which are synthesized and polymerized within specialized organelles called melanosomes. Detection of melanosome formation provides reliable functional evidence for melanocyte lineage maturation (Hearing, 2005). To determine whether IR induces melanosome formation in MSCs, first we used transmission electron microscopy (TEM) to establish a method for the ultrastructural analysis of Dct-lacZ$^+$ cells in the bulge area. Dct-lacZ$^+$ cells contained β-galactosidase reaction products deposited on the nuclear membrane (Figures 5G–5J). The cells were small in size and did not contain any melanosomes in the absence of IR treatment (Figure 5I). In contrast, IR treatment induced abundant melanosomes in Dct-lacZ$^+$ cells (EPMs) (Figures 5L and 5N). Melanosome maturation proceeds sequentially in a stepwise manner from stage I to stage IV during the process of melanocyte differentiation and is mediated by MITF target genes (Hearing, 2005). It is notable that typical stage II–III melanosomes (Figure 5N, arrows and arrowhead), which are found only in melanin-synthesizing melanocytes but not in keratinocytes, were present in addition to abundant stage IV melanosomes in EPMs. This finding provides functional evidence of melanocyte maturation with EPMs. Furthermore, the melanosomes in EPMs were indistinguishable from those in physiologically differentiated melanocytes in the hair matrix of mid-anagen hair follicles (Figures 5N and 5O). These findings, in combination with the chronological fate analysis of Dct-lacZ$^+$ cells in the bulge, demonstrate that MSCs in the niche undergo differentiation in response to IR to become pigment-producing dendritic melanocytes through melanosomal maturation.

IR-Induced Melanogenesis Depends on Mc1r but EPM Loss Does Not

The murine recessive yellow allele (Mc1r^e) is a loss-of-function mutation in the MC1R for MSH, which results in yellow hair color